OBJECTIVE LENS FOR A MINIATURE ENDOSCOPIC CONFOCAL MICROSCOPE

By

Nabil El Ferradi

A thesis submitted in partial fulfillment
of the requirements for the degree

of

Masters of Science

in

Electrical Engineering

MONTANA STATE UNIVERSITY
Bozeman, Montana

January, 2005

APPROVAL

of a thesis submitted by

Nabil El Ferradi

This thesis has been read by each member of the thesis committee and has been found to be satisfactory regarding content, English usage, format, citation, bibliographic style, and consistency, and is ready for submission to the college of Graduate Studies.

Dr. David Dickensheets

Approved for the Department of Electrical & Computer Engineering

Dr. James Peterson

Approved for the College of Graduate Studies

Dr. Bruce McLeod

STATEMENT OF PERMISSION OF USE

In presenting this thesis in partial fulfillment of the requirements for a master's degree at Montana State University, I agree that the library shall make it available to borrowers under the rules of the library.

If I have indicated my intention to copyright this thesis by including a copyright notice page, copying is allowable only for scholarly purposes, consistent with "fair use" as prescribed in the U.S. Copyright Law. Requests for permission for extended quotation from or reproduction of this thesis in whole or in parts may be granted only by the copyright holder.

Nabil El Ferradi

Dcember, 2004

ACKNOWLEDGEMENTS

The successful completion of this project was the cooperation of so many people, of whom the advice, encouragements and patience were indispensable.

First, I am grateful to my advisor Dr. David Dickensheets. His guidance, support, and a rare tact and patience in dealing with people made this project a great learning experience, on the academic level as well as on the human level.

I would like to thank each member in my group, Micro-Optics and Imaging group, for being patient and helpful whenever I needed help, with special thanks to Phil Himmer, whose experience was vital during the microfabrication phase. Randy True of SNF for his priceless help with the microfabrication.

I would like to thank Dr. Joe Shaw and Dr. Todd Kaiser for their advice and for serving as members of my graduate committee.

I would like to thank my parents, Driss and Sakina, for their care and still ongoing sacrifices to support me.

Most importantly, I am thankful to God, for the blessings of a sound belief in him, health, and sanity and for making me in the course of this life meet people who have been kind with me.

TABLE OF CONTENTS

TABLE OF CONTENTS - CONTINUED

LIST OF TABLES

LIST OF FIGURES

Figure Page

LIST OF FIGURES - CONTINUED

Figure Page

ABSTRACT

This thesis presents the design and testing of a micro-objective lens for a miniature endoscopic confocal microscope. The advance of confocal endo-microscopy for *in-situ* imaging can lead to considerable improvements in inspection, analysis, and diagnosis, especially in the biomedical field. The dimensions of the objective lens developed are 4.0 mm long and 2.0 mm in diameter incorporated into a probe that is 2.0 mm in diameter and 10.0 mm long. The size of the probe will allow it to be inserted in some of the smallest channels in an endoscope. The objective lens features a 0.33 numerical aperture, a 4x magnification, and 200 µm field of view and a sub-micron spot size. The optical system is compensated at two wavelengths, 488 nm and 515 nm. Chromatic and spherical aberrations are minimized through the use of 3 refractive plano-convex elements and an 8-level fused silica diffractive optical element. Details of the lens design, its simulation using computer ray tracing software, fabrication of the diffractive optical element and experimental characterization of the assembly are presented.

CHAPTER ONE

INTRODUCTION

Confocal Microscopy

As a minimally invasive imaging modality, endoscopy is widely employed in *in-vivo* medical imaging. The endoscope permits visualization of tissue at a macroscopic level, and is used to identify suspicious areas according to their appearance. Diagnosis of disease requires sampling of the tissue with a biopsy forceps and imaging the removed tissue under a microscope. Endo-microscopy refers to the use of a special endoscope to visualize tissue at the microscopic scale directly *in-vivo*. To image the tissue below the surface and to provide 3-D images, confocal microscopy may be employed [1]. We will refer to confocal microscopy delivered using an endoscope as confocal endo-microscopy or CEM.

In this way, instead of taking individual samples from their native environment to image on a microscope, the microscope is taken to the samples in their own environment, *in vivo*. To achieve such a goal, a confocal scanning microscope with illumination delivered through an optical fiber is used. This instrument is called the confocal microprobe [2].

Confocal endo-microscopy (CEM) has the potential for significant improvement in the inspection, analysis, and diagnosis of disease within intact tissues in their natural environment. The emergence of CEM will lead to new applications, such as surveillance of inflammatory diseases, monitoring and managing structural changes caused by disease processes, evolution of transplants on the cellular levels, and possible transplant rejections. Noninvasive *in-vivo* CEM could accelerate diagnosis, by providing real-time information and would permit more sample sites since the tissue is not removed. It also makes it possible to study tissues without artifacts that can be caused by fixation, sectioning, mounting, and staining.

In confocal microscopes light is focused on one spot on the specimen, while conventional microscopes illuminate the entire field of view of the specimen [3]. The light emitted back emanates either directly from the specimen or commonly from a fluorescent chemical marker used to stain the specimen. Figure 1.1 shows how the light reflected from the focused spot on the specimen is focused again and passes through a pinhole aperture carefully positioned in front of the detector to block light from out-of-focus planes. The blocking is done when light originating from a focal plane above the target plane focuses behind the detector's pinhole and is then not detected as most of the light hits the pinhole edges. In a similar fashion, light originating from a lower focal plane focuses and expands before reaching the aperture. This configuration helps reject light originating from overlying and underlying focal planes and gives the microscope its confocal property; it also makes it possible to optically image the specimen thin sections, a process called optical sectioning. Scanning a plane at a given depth results in a two-dimensional optical section at that depth, which is done successively at different depths to obtain confocal images that are stacked to form a three-dimensional image, thereby bypassing the limitations of blur and scatter present in conventional microscopy of thick samples, and allowing surface and sub-surface imaging.

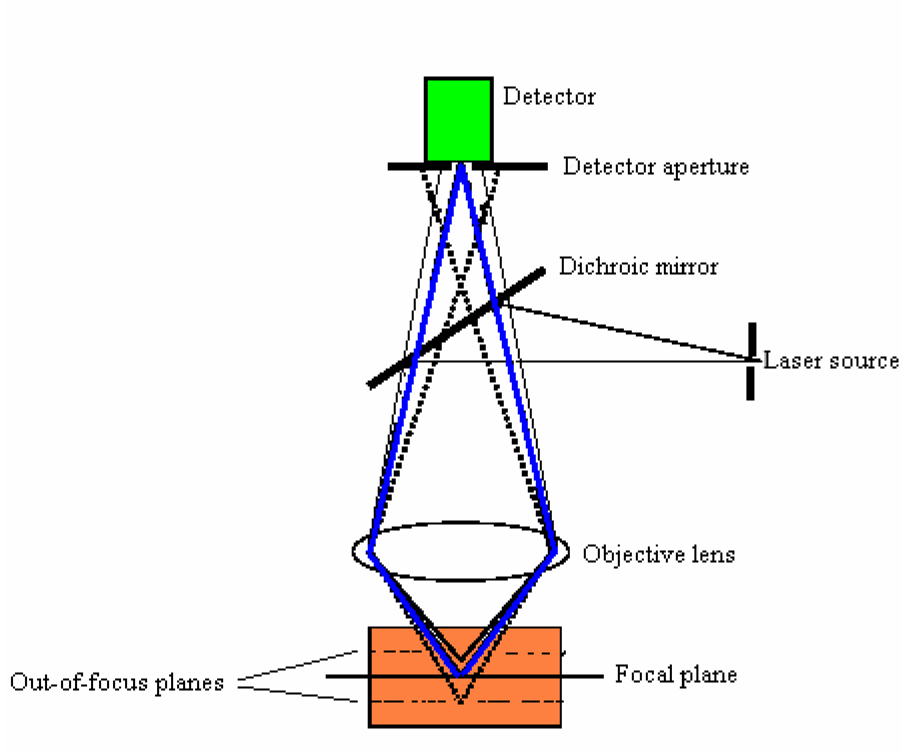

Figure 1.1: Ray paths in a confocal microscope

In Confocal Laser Scanning Microscopes (CLSM), instead of illuminating the entire specimen, light is scanned onto the specimen dot per dot and the light emitted is de-scanned dot per dot. Light is then passed through a pinhole to reach a detector such as a photomultiplier tube (PMT).

A confocal system can be characterized by its resolution, which is its ability to distinguish closely spaced points. Axial resolution in the direction of the optical axis R_{axl}, and lateral resolution in the transverse plane R_{lat}, are given by [4]

$$R_{axl} = \frac{0.9\lambda}{NA^2} \qquad (1.1)$$

$$R_{lat} = \frac{(0.37\lambda)}{NA} \qquad (1.2)$$

with the design wavelength λ

and $NA = n \sin\alpha$ (1.3)

and α the half-angle within which light is accepted.

Lateral resolution is inversely proportional to the NA, while axial resolution is inversely proportional to the square of the NA.

It is worth noting that to improve the resolution of the optical system, the design wavelength could be chosen to be smaller, or simply a larger NA could be chosen, which would improve the resolution laterally and axially and give better light collection capability as can be seen in figure 1.3. A more detailed discussion will follow in chapter two.

Fluorescence

In fluorescence, a molecule is excited to an elevated electronic energy state by absorbed photons, and then relaxes to a lower energy state before undergoing radiative decay back to the ground state. The radiated photons have less energy and a longer wavelength than the excited photons. Therefore, the excitation and absorption peaks do not coincide, but are separated by an amount called the Stokes shift [5]. Spatial resolution will be determined by both the excitation wavelength and also by the emission wavelength. Confocal fluorescence imaging has been thoroughly described in the literature [4].

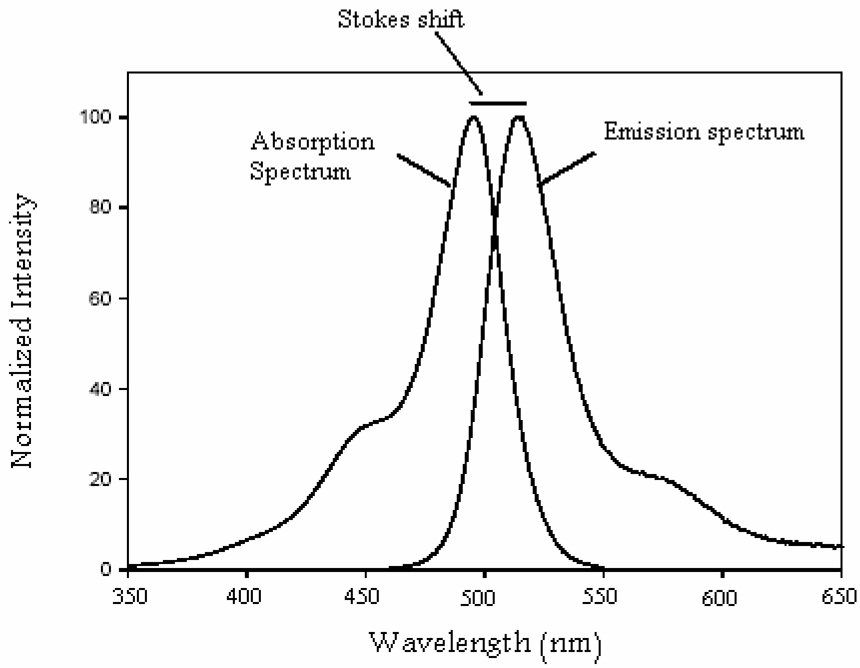

Figure 1.2: Stokes shift in solution at 488 nm and 515 nm

An increase in the size of the detector aperture decreases the resolution, as more out-of-focus light reaches the detector. The signal intensity is increased while faculty to differentiate between different planes decreases. Choosing the aperture size to be close to the Airy disk is the best solution to optimize the resolution and light collection performance as it will be at the limit of the Rayleigh criterion. In our application the pinhole is replaced by the core of a single-mode fiber. Confocal imaging with optical fiber has been treated in the literature [6] [7].

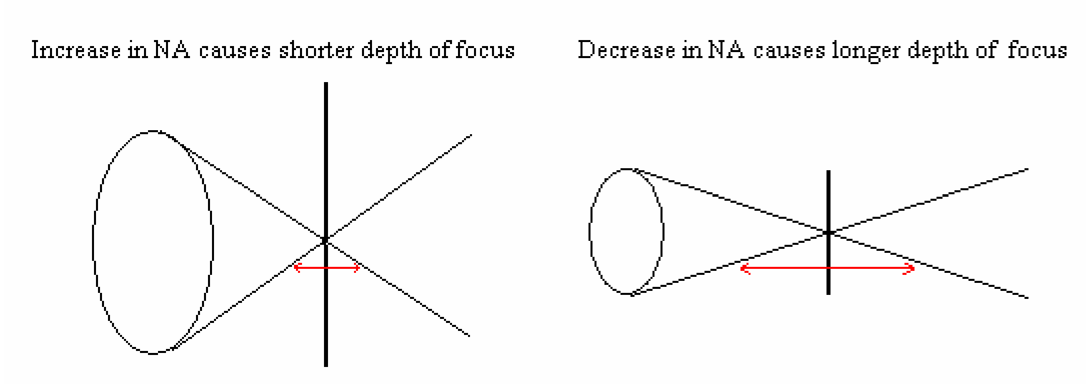

Figure 1.3: Effect of NA on axial resolution

In-Vivo Confocal Microscopy

A limitation of confocal microscopy is the requirement that samples to be studied need to be placed directly under the instrument. The measurement setup alters the sample for the simple reason that the actual observation is done outside the natural environment. A concrete example would be the use of confocal microscopy in the study of skin vasculature with blood flow, with unique advantages of *in-vivo* imaging such as avoidance of dehydration, fixation and staining of the tissue [7].

A primary challenge for *in-vivo* microscopy is miniaturization of the instrument to permit access to sites of interest. To address this challenge, a confocal microscope was designed and built with the capability of real-time scanning laser confocal microscopy in a package small enough to be inserted in the working channel of an endoscope.

Microprobe Description

In this thesis the design, fabrication and assembly of multiple parts of a microprobe for use in endoscopic applications, with a diameter not exceeding 2.0 mm and length less than 10.0 mm is described. The NA of the system would be 0.33, with a magnification of approximately 4x, a sub-micron spot size, and 90 degrees field of view. The optical system would optimally operate at two wavelengths, 488nm and 515nm to allow for fluorescence imaging using fluorescing dye. The objective lens will be a set of adjacent lenses, a refractive system and a diffractive optical element (DOE). The lenses are to be packaged in a 2.00 mm fused silica tube combined with a MEMS tip-tilt and deformable mirror in front of the DOE for scanning as well as focus control and aberration compensation.

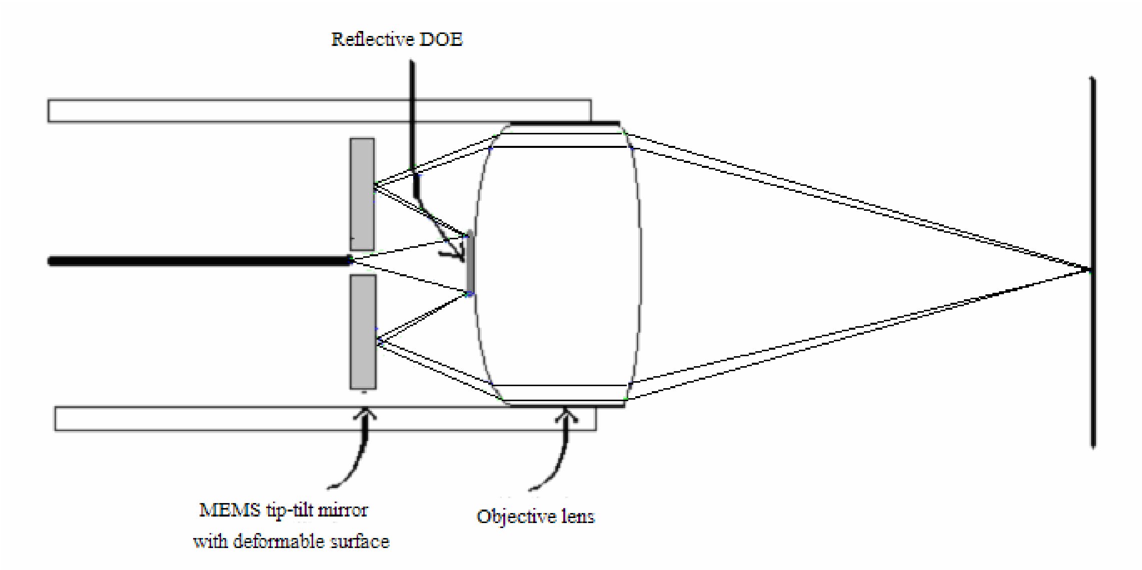

Figure 1.4: Axial probe architecture

Thesis Overview

In this thesis I describe the design and testing of a micro-objective lens for the miniature endoscopic confocal microscope.

Chapter two presents the objective lens design. It gives a description of the microprobe and dimensions of the lenses and the packaging. This chapter discusses different aberrations, undesired optical effects and theoretical performance. Chapter three introduces the design of the diffractive optical element in detail. The different steps involved in the design and microfabrication are discussed with diffraction efficiency test results. Chapter four presents the experimental lens characterization, the measurements are compared to theoretical expected results. Finally, in chapter five conclusions are drawn and potential system improvements are suggested.

CHAPTER TWO

OBJECTIVE LENS DESIGN

Introduction

The optical system needs to behave similarly when emitting light to excite a sample, and be able to collect light back upon excitation of the sample with the same efficiency. Chromatic aberrations play an important role in image quality, if excitation wavelength and emission wavelengths do not share a common focal point, the detector will exclude an important amount of emitted light, as it will seem to come from an out-of-focus plane. Another important issue is that of spherical aberration, which arises as the microscope focuses deeper in the sample.

In a traditional attempt to compensate for chromatic aberrations, negative elements which offer higher dispersion can be used. By grinding the edges of a known standard radius ball lens it is easy to make a plano-convex lens whose radius of curvature is that of the ball lens, with a flat polished on its side. Grinding ball lenses to make negative lenses was not an option for the lens manufacturer. There remains the need to cancel out the positive dispersion of the positive elements. Positive diffractive optics have an opposite dispersion than that of refractive lenses so our design incorporates a DOE for chromatic balancing.

A DOE is a multi-level phase relief that modulates the wavefront to give the desired phase profile [10]. One of the disadvantages usually associated with diffractive optical elements is their wavelength discrimination, meaning they would optimally operate at the designed wavelength and present serious distortions and dramatic decrease of diffraction efficiencies at other wavelengths. This property is used to advantage in the optical system to compensate chromatic dependence of the refractive optical components in our system. A DOE has been designed, fabricated, and tested to work optimally on 2 distinct wavelengths (or more practically on a range of wavelengths 488nm –515nm). Because of the design freedom of the DOE, we can make that element aspheric to compensate other spherical aberration in our system to arrive at a compact, high performance lens.

Objective Lens Description

The objective lens design is illustrated in figure 2.1. Lens L3 primarily collimates light emerging from the fiber. Two additional lenses, L3 and L2, form a pseudo-aplanatic front, which allows the convergence of rays to be increased without introducing spherical aberration or coma [8]. The addition of the DOE in combination with the other optical elements should be able to compensate for chromatic, residual spherical aberrations and coma. From the assembly perspective, being able to separate lenses by precise distances (air gaps between surfaces) would be a challenging task knowing the miniature sizes of the optical components, so during the design process the lenses were assumed to be in contact. The optimization process then was used to set the lengths of the lenses, and the radii were chosen from a subset of fixed available ball lens radii.

The objective lens is extremely compact. It is a set of 4 lenses, 3 of which are refractive plano-convex and one diffractive binary optical element.

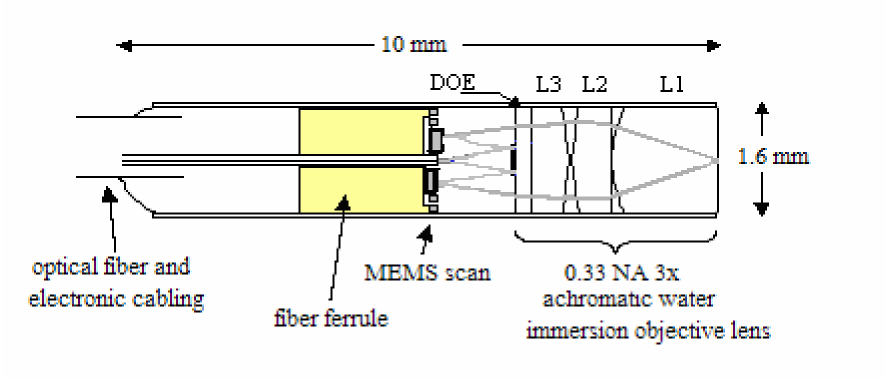

Figure 2.1: Endoscopic confocal microscope

Optimax Systems Inc., New York, manufactured the refractive plano-convex ball lenses. The DOE was machined in fused silica. Fused silica was a good candidate as substrate for the DOE because it can be used from near infrared to deep UV wavelengths, and mostly because its amorphous structure allows it to be etched accurately and uniformly. The DOE was designed and fabricated in two trials. A first trial took place at the Cornell Nanofabrication Facility (CNF). The second trial was done at the Stanford Nanofabrication Facility (SNF). The fabrication at SNF was more suited for transparent substrates as the facility went through transformations in which almost all of the machines have been upgraded to be able to accommodate transparent substrates, but still the process did not proceed without complications. The detailed steps of the design and fabrication of the DOE are included in chapter three and four.

Aberrations

The main goal of the design was to obtain an optical system with a sub-micron laser spot size over a depth range from 0 to approximately 100 µm and a field of view of

200 µm. Such a design requires control over aberrations. The primary limiting ones are spherical and chromatic aberrations and a combination of both.

Spherical Aberration

Spherical aberrations occur when all the rays do not focus to a single point. Rays closer to the edge fail to focus in the same location as rays closer to the center of the structure [11]. Therefore, off-axis rays are brought to a focus closer to the lens compared to on-axis rays if the spherical aberration is positive, further from the lens if negative. Longitudinal spherical aberration is the distance along the optical axis between the intercept of paraxial rays and the marginal rays while transverse spherical aberration is the height at which marginal rays intercept the focal plane.

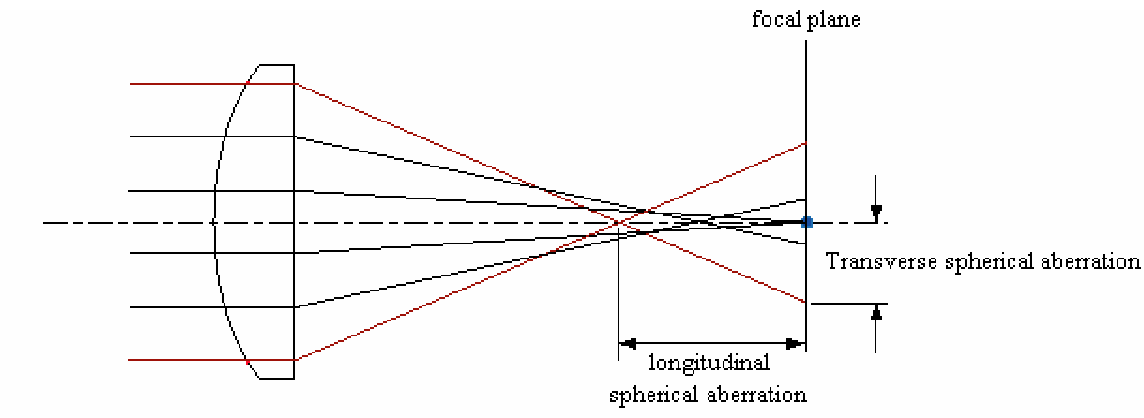

Figure 2.2: Longitudinal and transverse spherical aberration

Chromatic Aberrations

Rays of different wavelengths are refracted at different angles because of the dependence of the index of refraction on the wavelength. The index of refraction in most materials is inversely proportional to the wavelength, so shorter wavelengths will come to a focus closer to the lens than will longer wavelengths will [11]. The distance along the optical axis between different wavelength focal points is referred to as longitudinal chromatic aberration.

In a diffractive lens, the power of the lens depends on diffraction, which is greater for longer wavelengths. Therefore, the power of a diffractive lens decreases for shorter wavelengths. We will use the chromatic aberration of the DOE to balance the chromatic aberration of the refractive elements. In addition, because the phase function of the DOE is defined lithographically we can give it an aspheric phase profile to compensate residual spherical aberrations.

The third function of the DOE is the retro-reflecting mirror to accommodate folded beam path of co-axial architecture. All accomplished with one DOE

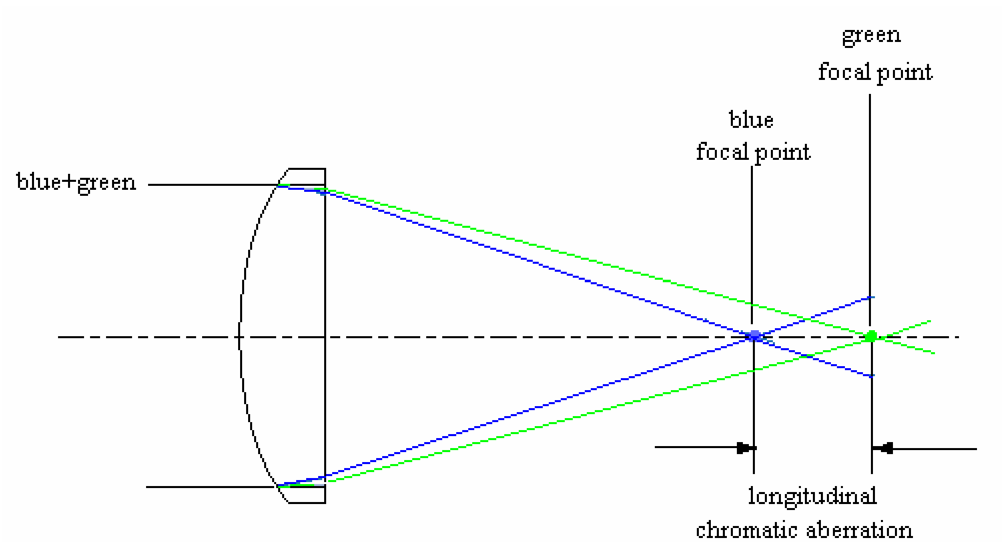

Figure 2.3: Longitudinal chromatic aberration

<u>Objective Lens Assembly</u>

The assembly and packaging of the microprobe have been some of the most challenging and time consuming phases of the entire process due to the minuscule nature of the components. InnovaQuartz Inc. of Arizona made fused silica chamfer ferrule that were 1.605 mm inner diameter, 2.000 mm outer diameter and 10.0 mm long to be used as housing for the lens assembly. Initially we have thought of taking advantage of the chamfer as a means to ease the insertion of the lenses inside the tube, later it turned out that it was not necessary.

First the DOE had to be paired with L3, which was done using an adhesive commonly used in optics. We used UV16, a UV-curable epoxy resin purchased from Master Bond Inc. NJ. UV16 was chosen for its optical properties as its index of refraction is 1.517 and is ultra-low viscosity (120-150 cps) with less than 2% shrinkage upon cure. The ultra-low viscosity was instrumental in obtaining the thinnest film of epoxy between L3 and the DOE. The epoxy was wicked in between the two surfaces by bringing a minute drop of UV16 at the interface between the two components, then the liquid expanded between the two surfaces and occupied the empty spaces. After that, the two lenses were very carefully aligned, using translation stages, and then exposed under a mercury lamp long enough for the epoxy to cure (5 minutes). As the epoxy was very resistant to solvent and isopropanol, the glued lenses were immersed in a bath of acetone and isopropanol respectively for 30 minutes to clean them from any residues accumulated during the process. The two lenses were carefully introduced in the fused silica tube, then the rest of the lenses were pushed against them and introduced deeper inside the tube. There was almost no need to align the lenses inside the tube because of the very high tolerance of the radii of the lenses and the fused silica tubing (±5 μm). The tip of L1 was intentionally left outside the tube so that we could have the option of touching the sample and imaging at the interface. We applied once more the UV16 curable epoxy between L1 and the tube to seal the part of the probe directly in contact with water, the technique that was used was the same as the one used to glue L3 to the DOE. The MEMS scanning mirror is a deformable mirror which adds some additional control for focus and spherical aberrations, the design of this mirror was a separate project.

Zemax Simulation

Zemax is a ray tracing simulation tool, which helps model, analyze and design optical systems. Zemax was used to optimize the design for minimal spot size, and reduced chromatic and spherical aberrations.

The model included 3 refractive elements, a DOE, and a MEMS mirror. At the starting of the optimization process the variables were: lens thickness, radii of curvature, and coefficients for the DOE phase function. The model was made more practical to assemble by setting the lens separation to zero so that the lenses are in contact with each other. The refractive lenses were chosen to be plano-convex because of the process of lens grinding process. The assumption was to start with ball lenses with preset radius of curvature that would be polished and a flat could be easily formed on its side. The freedom was given initially to the software to optimize radii of curvature, then the closest standard off-the-shelf radii were picked. Then we chose dimensions for the 3 plano-convex lenses that were not excessively stringent to manufacture. The lenses material was not optimized for as there was only a few available choices from the lens manufacturer. Using simple microscope objective design consideration as starting point, the merit function was used to solve for minimum wavefront errors, minimum optical path difference, lateral and axial color, as well as spherical aberrations. The Zemax merit function is provided in appendix A. The next step was to give more freedom to the simulation software to model the diffractive element. We came out with three different designs. As the DOE is defined by a polynomial phase function that we translated to phase profiles with known depths and features, the design that best simulated the MEMS scanning mirror and suggested curvatures that the actual fabricated mirror could reach was chosen, a range of ±5 degrees mechanical tilt and a maximum of 5 μm center deflection. The attributes of the MEMS mirror allow for scanning the beam in a plane and changing the depth of focus at need. The effective focal length of the system being 1.25mm.

Table 2.1 details the properties of the refractive and diffractive lenses used in the objective lens

Lens	Material	n	Diameter /tol	Thickness /tol	Radius of Curvature /tol
L1	LASFN9	1.850	1.600 /-0.005 mm	2.200/-0.005 mm	1.500/-0.005 mm
L2	BK7	1.517	1.600/-0.005 mm	0.650 mm	3.500/-0.005 mm
L3	BK7	1.517	1.600/-0.005 mm	0.650/-0.005 mm	2.500/-0.005 mm
DOE	Fused Silica	1.464	1.600 mm	0.500 mm	$-591.1r^2+174.22r^4$

Table 2.1: Lens specifications

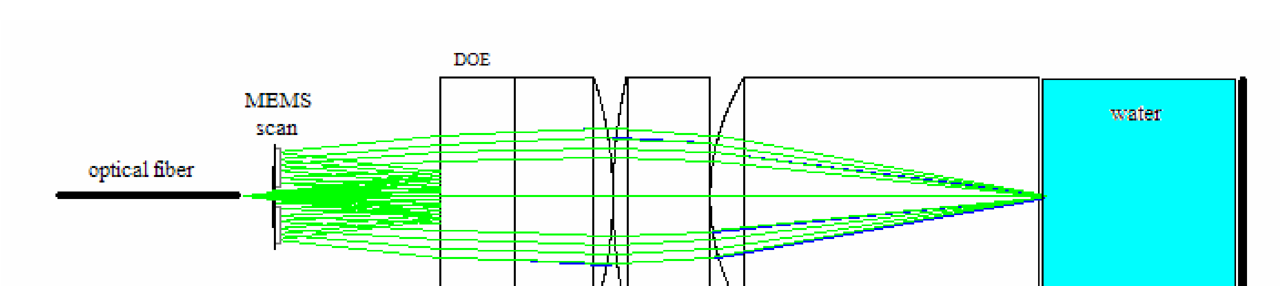

Figure 2.4: Objective lens Zemax 2D layout

CHAPTER THREE

DIFFRACTIVE OPTICAL ELEMENT DESIGN AND TESTING

Introduction

There is an increasing demand on miniaturization and integration in the optics field. The main goals are pushing toward a decrease in the weight, the size, the power usage, the maintenance and the cost of optical systems. Diffractive Optics plays an important role in helping achieving these goals offering light weight and potentially aspheric replacements for refractive lenses. Additionally diffractive optical elements offer unique capability in beam forming adding flexibility to optical system design.

DOEs have multiple applications in optics because of their compactness and their high potential for aberration correction. DOEs have been made very compact with the improvements in the micro-fabrication technology, optical microlithography in particular, as well as ray tracing software and computer aided design (CAD) tools. The main difference between a "classical" optical element and a diffractive one is that the design of the classical optical element is based on the refraction of light, essentially using Snell's law, while the diffractive element design is based on the diffraction of light from a surface on a grating and is thus described by grating equations. For refractive optical elements the power depends on the curvature of the surfaces and the change in the index of refraction at interfaces, while in a diffractive element the power depends on the grating constant and the design wavelength. One of the reasons for choosing a diffractive element over a refractive element is that the DOE can be made thinner compared to a Refractive

Optical Element (ROE), because in a DOE there is no difference between a 2π and a p2π delay due to the periodic nature of the electromagnetic wave (p being any integer), assuming nearly monochromatic light.

For our application we will use the wavelength sensitivity of diffraction to balance the chromatic aberration of the other refractive lenses elements to create an achromatic lens.

The modeling of a DOE relies on the dimensions involved. Ray tracing, using scalar diffraction theory, is a standard method for designing DOEs. In the case where the incident light wavelength is comparable to or larger than the minimum size of the DOE, the DOE might be treated as a thin phase modulating plate where the incident wavefront is retarded and its propagation can be modeled using scalar diffraction theory. However, in the case where the incident wavelength is much larger than the DOE's minimum feature size, rigorous electromagnetic theory should be used to predict the performance of the DOE [12]. Our design wavelengths are 488nm and 515nm while the smallest feature size of the DOE is 1.30μm and has a period of 10.72μm, which comfortably fits in the scalar diffraction theory.

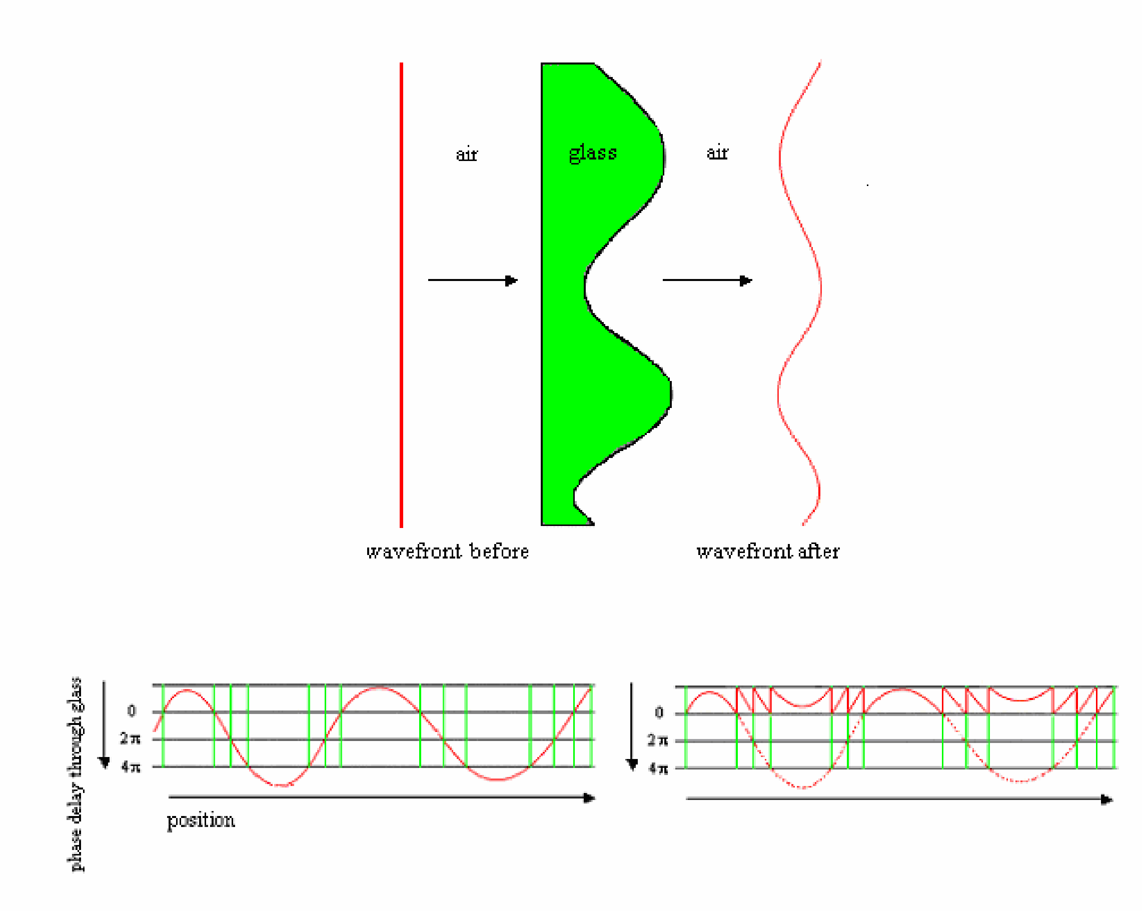

Figure 3.1: Continuous piecewise structure showing an upward shift modulo-2π

Figure 3.1 shows how a DOE can modulate a wavefront taking advantage of the periodic nature of the wavefront to minimize the thickness of the substrate, glass in this case. Figure 3.2 shows how the resulting optical wave is modulated by a thin DOE.

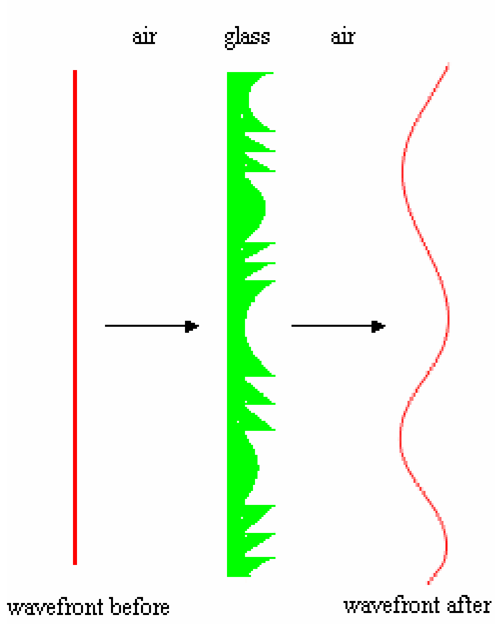

Figure 3.2: Wavefront modulation by a diffractive optical element

DOEs can have continuous microreliefs or multiple level microreliefs (‘binary optics’). The diffraction efficiencies are determined by the phase modulation depth and the profile shape. The multiple-level approach arises from early experiments in which the continuous blaze was approximated to a stepped quantized profile [13]. The phase function expression is continuous and needs to be processed to yield to surface relief heights. The phase profile is quantized into N discrete phase levels to simplify fabrication, which approximates the curved phase shape to a staircase profile with $2\pi/N$ step height, N being the number of steps.

The quantized approximation eases difficulties due to fabrication of continuous phase shape. The stepwise approximation of the phase profile makes it possible to use VLSI techniques to create complex shapes such as spherical, parabolic and other surface profiles.

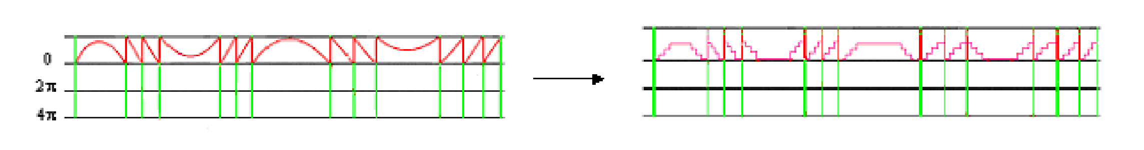

Figure 3.3: Example of the transition from blazed to a 4-level phase profile

Swanson, of MIT Lincoln Laboratory, demonstrated through a binary coding of the phase profile that efficient DOEs could be fabricated using CAD and VLSI fabrication techniques. The work done at the Lincoln Laboratory increased the number of phase levels formed in N process steps from N+1 to 2^N, which was a giant leap that would drastically reduce the cost of fabrication and make it easier to fabricate higher diffraction efficiency devices in fewer steps mainly avoiding cumulative errors associated with an increased number of masks. The 2^N step structure is fabricated by a succession of N sets of photolithographic and dry-etching processes by use of N different mask patterns.

Fabrication of the Diffractive Optical Element

The fabrication of optical structures is simpler and less costly than VLSI processing, which involves complex successive cycles. A multi-level diffractive element is fabricated in a few steps that can be limited to photolithography followed by etching in cycles [10] [12] [13]. The mask pattern is exposed onto the substrate and the open regions are removed in each etching phase. For example, when the etching depth ratio is set to

4:2:1 corresponding to the three processes, if all the mask patterns are perfectly aligned one obtains an 8-level structure.

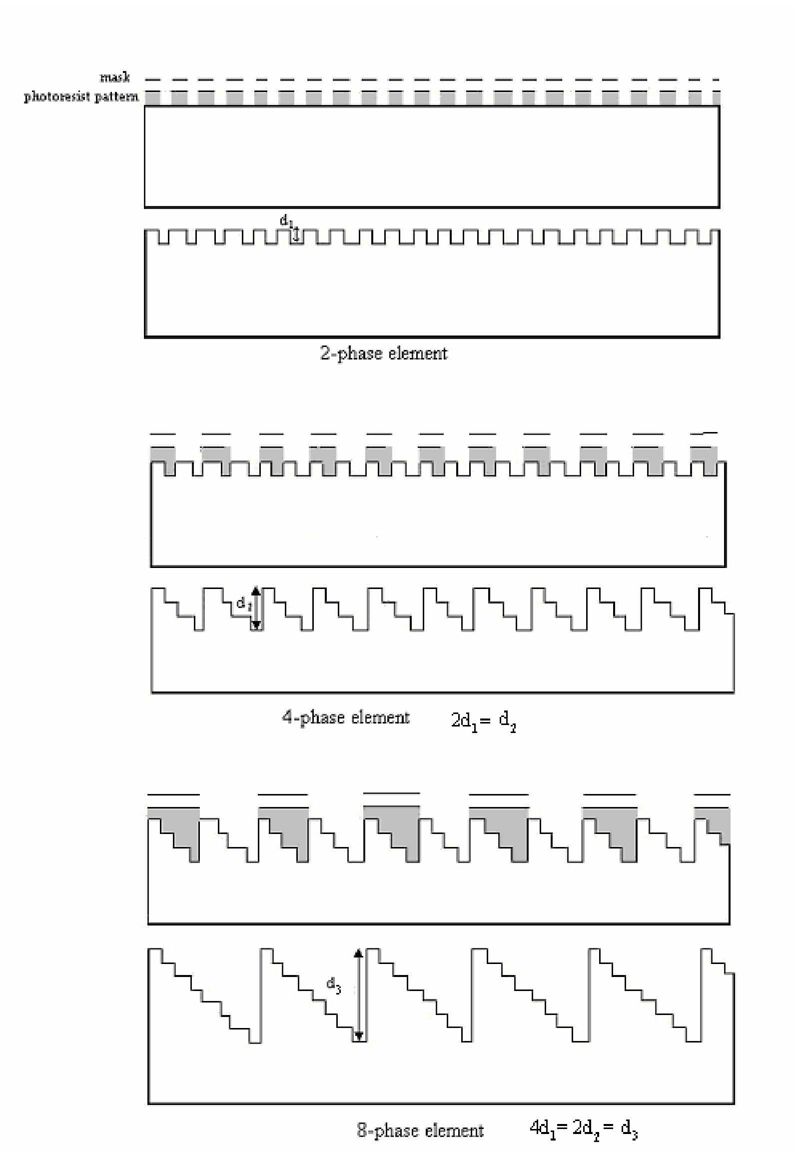

Figure 3.4: 8-Step phase relief formed by setting etch depth ratio to 4:2:1

The first mask creates a 2-level profile, and the following masks each doubles the number of phase level respectively with the etching depth doubling each time. The periodicity, similarly, doubles each time as will be detailed in chapter 4.

Diffraction Efficiency

The decision to make an 8-step binary optical element was taken for the reasons that will follow. The first order diffraction efficiency can be expressed as [10]:

$$\left|\eta_1\right|^2 = [\tfrac{N}{\pi}\sin\tfrac{\pi}{N}]^2 \qquad (3.1)$$

From equation 3.1 it can be seen that the higher the number of level the higher the efficiency, and as $N \to \infty$ the efficiency would approach 100%.

Following are sample of first order diffraction efficiencies for different quantization levels: $\left|\eta_{1,N}\right|^2$

N	2	4	6	8	10	12	14	16
η_1^N	0.405	0.811	0.912	0.950	0.967	0.977	0.983	0.987

Table 3.1: First order diffraction efficiencies η for N quantization levels

Figure 3.5 plots the 1st order diffraction efficiencies for an optimized N number of steps according to the scalar theory:

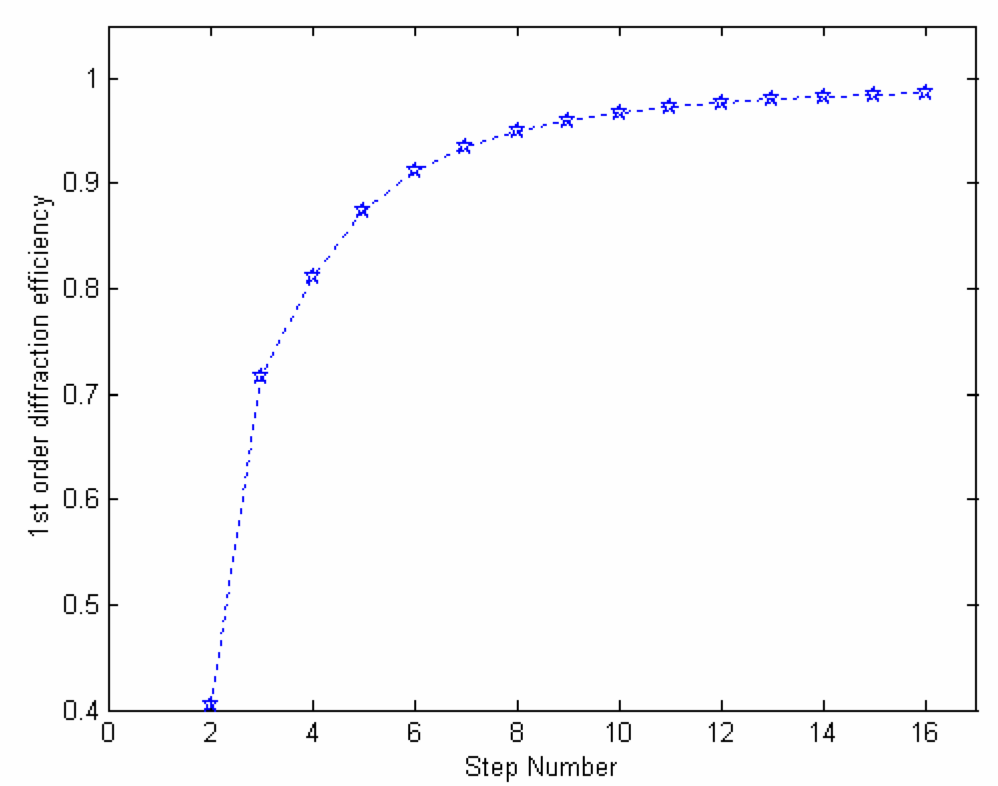

Figure 3.5: 1st order diffraction efficiency vs. step number

From N = 8 the efficiency values change very slowly and the graph flattens out. Going beyond 8-levels would increase the efficiency by only 5%. On the other hand, it would greatly increase the chances of mask misalignment and make the fabrication process less controllable not guaranteeing repeatability. Mask alignment errors, which have a dominant effect on the degradation of the DOE's performance, are cumulative as each additional fabrication step adds a further decrease to the DOE's performance. The machine we used for patterning the resist, Nikon NSR projection stepper, offered an alignment accuracy in the 0.18-0.25 µm range. If the number of masks is increased, relative mask alignment would get worse after each exposure.

As mentioned earlier in this thesis, the purpose of the DOE designed for the microprobe is to perform similarly at 488 nm and 515 nm. For a DOE 100% efficient (continuous relief) at λ_o for an m^{th} diffractive order at wavelengths different than the one designed for, the diffraction efficiency can be expressed as [12]:

$$\eta^2(\lambda)_m = [\frac{\sin\{\pi(\lambda_o/\lambda - m)\}}{\pi(\lambda_o/\lambda - m)}]^2 \quad (3.2)$$

so the overall efficiency can be obtained by combining equations 3.1 and 3.2. The 1st order overall diffraction efficiency for an N-step phase relief DOE is then:

$$\eta^2(\lambda)_{overall} = [\frac{\sin\{\pi(\lambda_o/\lambda - 1)\}}{\pi(\lambda_o/\lambda - 1)}]^2 \times [\frac{N}{\pi}\sin\frac{\pi}{N}]^2 \quad (3.3)$$

The 1st order diffraction efficiency was plotted with respect to wavelength in figure 3.6 to see the range for which the behavior of the DOE would be acceptable.

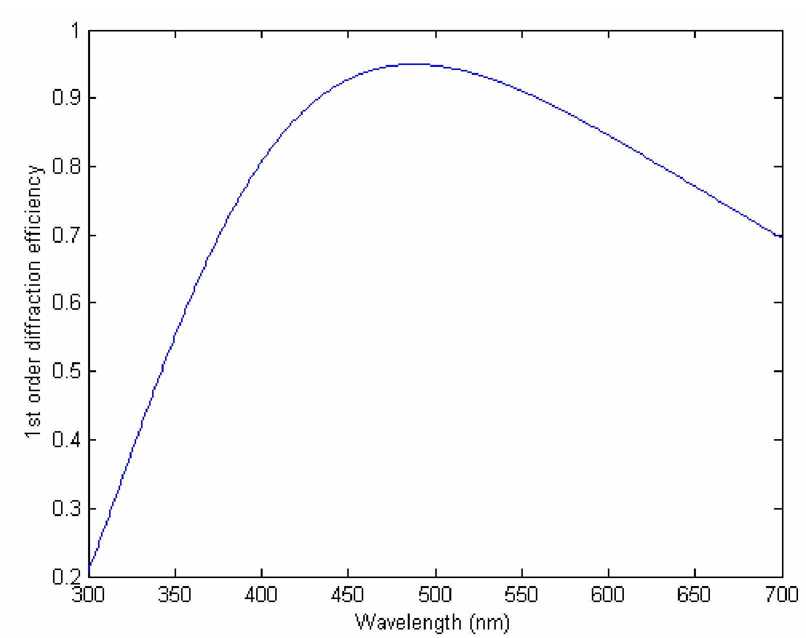

Figure 3.6: 1st order diffraction efficiency change relative to wavelength

Theoretically, the wavelength range for which the DOE would achieve 1st order diffraction efficiencies beyond 80 % diffraction efficiency would be the 400nm-625nm range, while 90% diffraction efficiency would occur in the 425nm-550nm range.

Phase Function and Quantization

The DOE can be specified by any arbitrary phase function. For a zone plate, the focal length and the design wavelength are sufficient; more general phase functions can be described by cartesian or radial polynomials or by Zernike polynomials. In Zemax, the defined phase function is in polynomial form. We chose to constrain the phase function to a fourth order equation in the radial coordinate *r* to allow for balancing primary chromatic, and spherical aberrations.

Zemax optimized for minimal PSF and to correct for aberrations such as chromatic and spherical aberrations. Zemax does not model the micro-structure of the DOE, instead it predicts the direction and the wavefront aberrations using phase polynomials, in function of the radius *r* of the DOE, with variable degrees whose coefficients can be manually changed or left to the software to optimize. It uses an actively damped least squares algorithm, which can be changed by changing operands in a merit function composed of weighted errors relative to target values. The final merit function is included in the appendix at the end of the thesis. After optimization Zemax proposed an optical element with the following phase function

$$\phi = -591.1r^2 + 174.22r^4 \qquad (3.4)$$

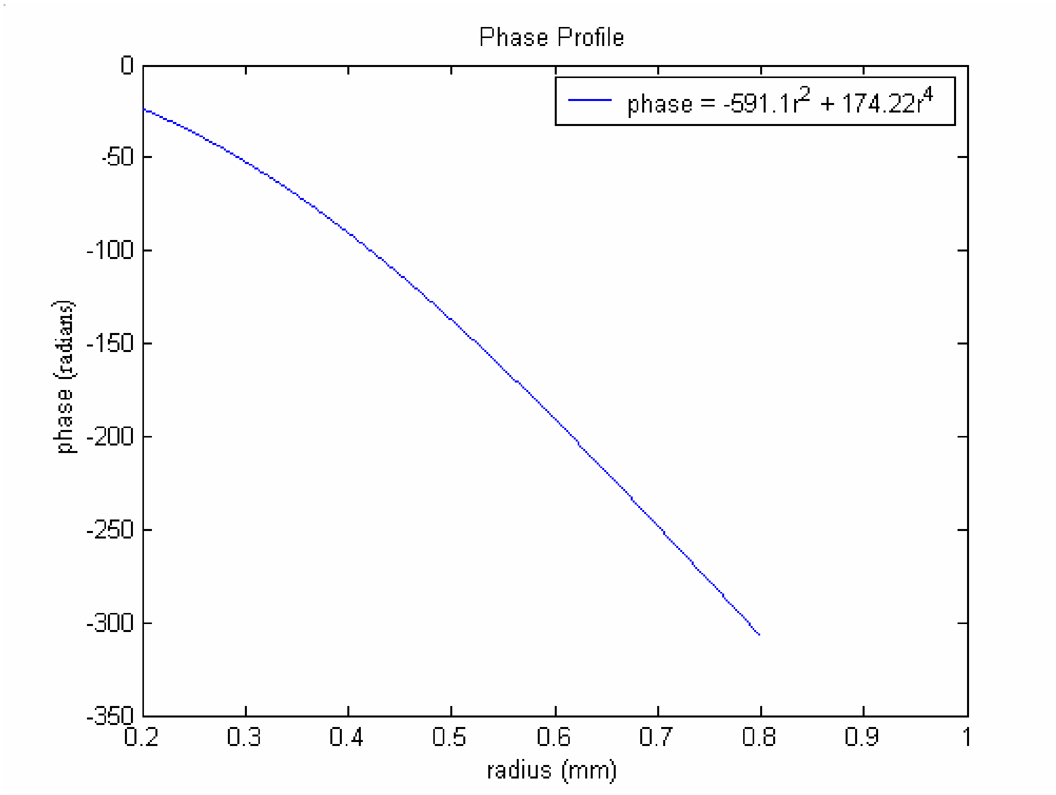

Figure 3.7: DOE phase function

In figure 3.7, which plots the phase function given in equation 3.4, one can notice that the larger the radius the steeper the slope. The reason for this is that the coefficient associated with r^2, which is just a focusing term modified by the r^4 term that minimizes spherical aberration.

Figure 3.8 is the same graph with the corresponding quantization superposed on it, notice that the origin of the graph is now shifted up to 0. The continuous phase function is quantized into discrete levels of height $2\pi/N$.

As demonstrated in [12], the optimum total depth for an N-level is $d_{opt} = \frac{N}{N-1}\frac{\lambda}{n-1}$.

For N levels, the individual step height is $d_{step} = \frac{\lambda_o}{N(n-1)}$, with λ_o being the design wavelength, and n the index of refraction of the DOE substrate.

In the design an 8-level DOE was chosen, so step heights are each 2π/8, in other terms d_{opt}/N.

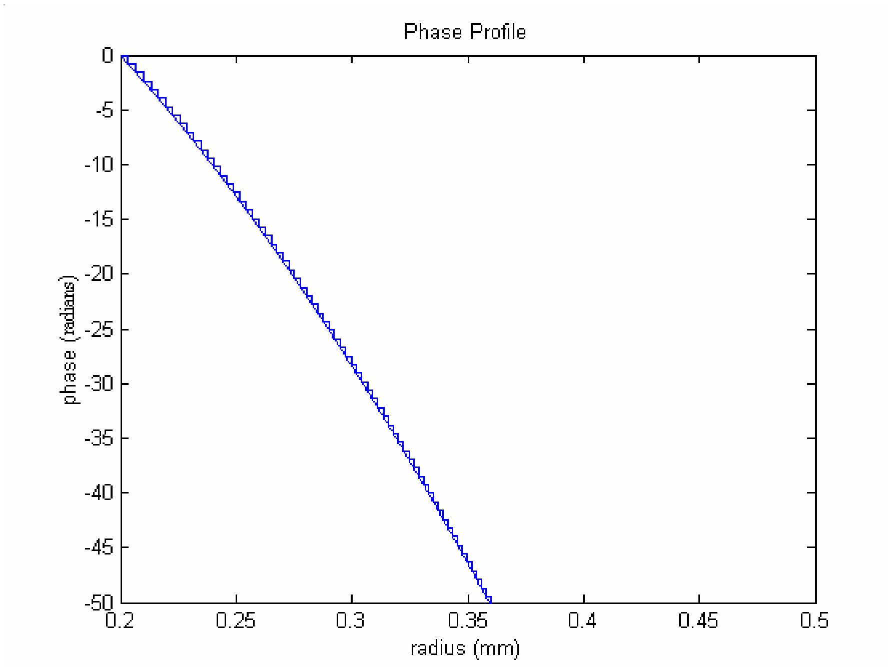

Figure 3.8: Quantized phase function

After the function is passed through a 2π delimiter at the design wavelength and quantized into discrete N steps, the phase profile adopts a staircase profile as shown in figure 3.8, which highlights a magnified portion of the quantized phase function. Only a portion is shown so that the reader can see the steps whose width at the lens perimeter is as low as 1.30 μm.

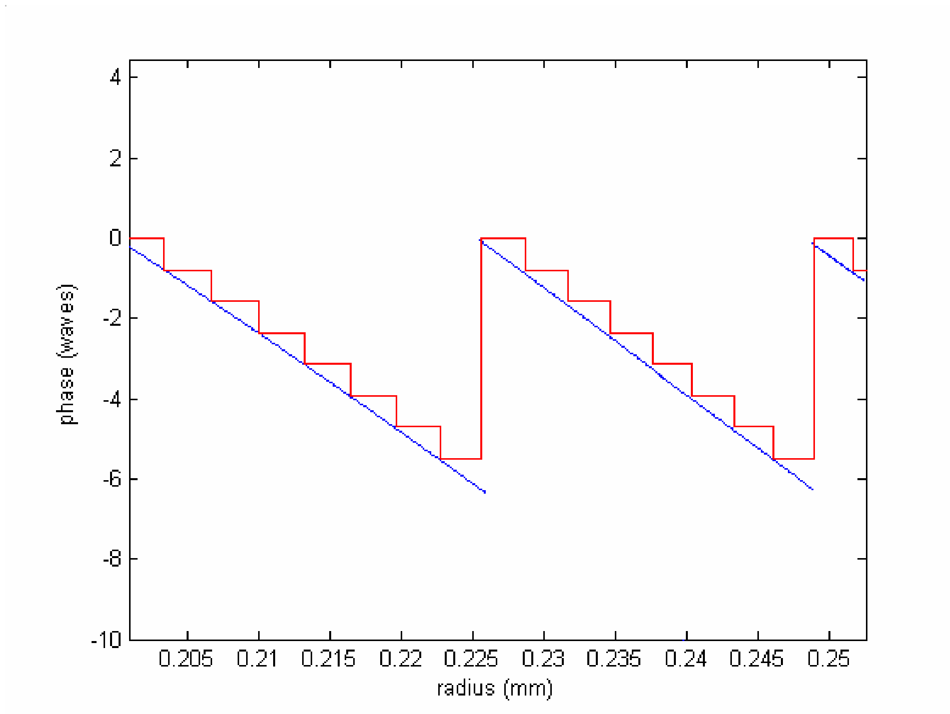

Figure 3.9: 8-level staircase

In our design, the primary wavelength is λ= 488 nm in fused silica with a refractive index of n = 1.46, so the optimum depth for an 8-step profile is d_{opt} = 945 nm. Individual step height is $d_{step} = \frac{\lambda_o}{N(n-1)}$ = 135 nm, meaning that the subsequent etch depths will respectively be 270 nm and 540 nm. If the primary design wavelength was 515 nm, individual step height would be 139 nm, similarly successive etch depth would be 278 nm and 556 nm, all of which are within 3% of the values obtained when the primary design wavelength is 488 nm. In addition to the small difference between the relief depths for the two wavelengths, one can see in the fabrication part that the tolerances associated with the microfabrication process will be included in the 3-5% bracket. The example of our 8-level fabrication resist patterning and etching is detailed in figure 3.10.

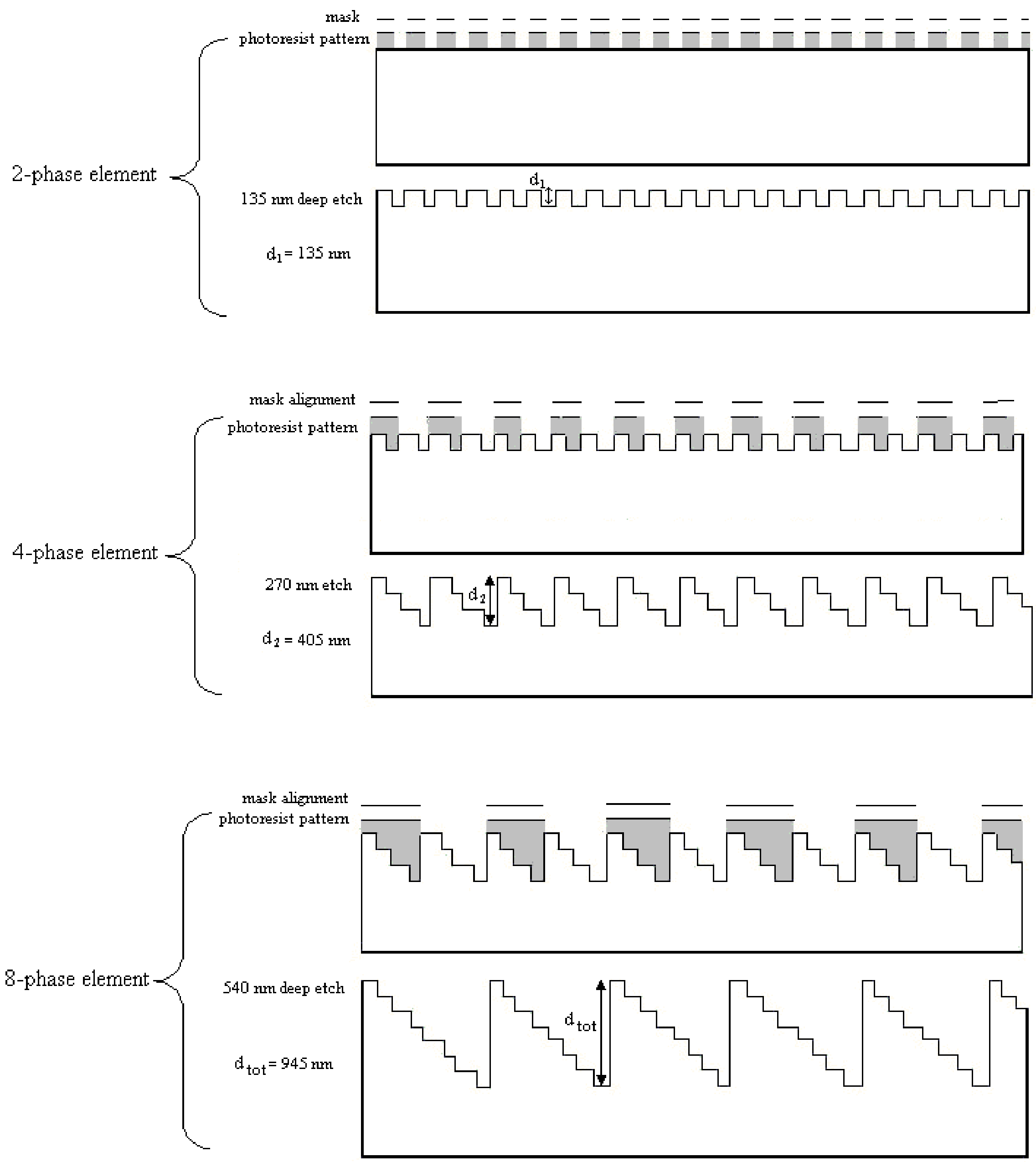

Figure 3.10: Fabrication steps of an 8-level DOE

The mask pattern is exposed onto the substrate and the open regions are removed in each etching process. The etching depth ratio is set to 4:2:1 corresponding to the three processes. If all the mask patterns are perfectly aligned one obtains an 8-level structure.

In case there are errors during the alignment one will encounter serious defects in the shape of the profile and end up with a step-like structure that includes ridges and trenches. Figure 3.11 shows an example of misalignment on the second mask, and we assume registration of the third mask is perfect, the result is an extremely irregular staircase profile.

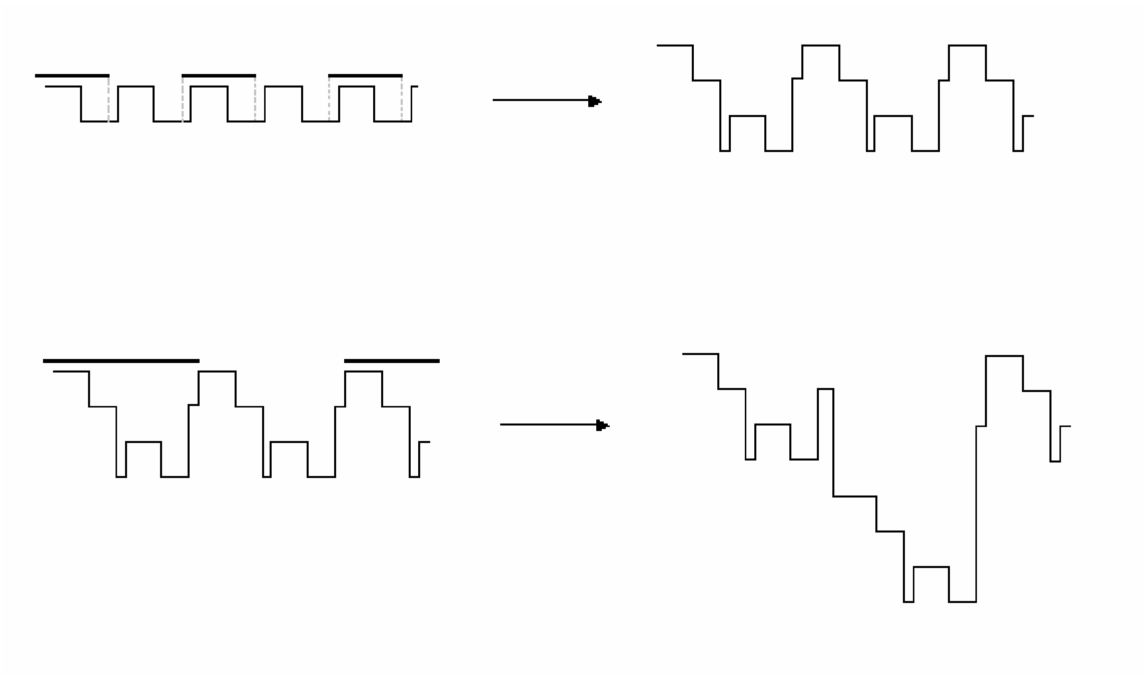

Figure 3.11: Misalignment effects on an 8-level DOE

In fact, misalignment would involve more serious shape anomaly, as it is practically impossible to misalign the second mask without making further errors in subsequent masks. Figure 3.12 shows an SEM of a device with the second mask misaligned. One can clearly see the trenches and ridges caused by the alignment error.

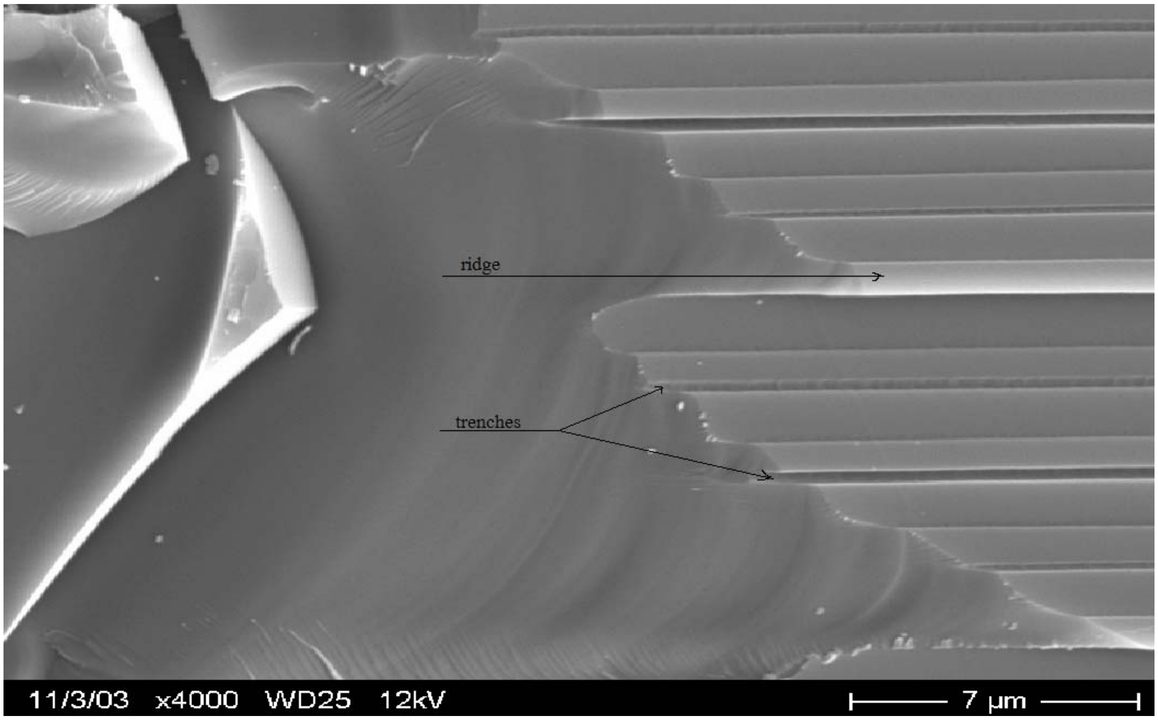

Figure 3.12: SEM of misalignment effects

The consequences of such profile error would be degraded optical performance resulting in intensity perturbation among different orders, which inevitably alters the diffraction efficiency [14].

Microfabrication Process

Micromachining uses techniques from semiconductor fabrication technology to create microns and sub-micron features. DOEs may be built using micromachining techniques developed for silicon processing.

Compared to silicon, glass offers a narrower range for micromachining processes, but on the other hand provides some unique features such as optical transparency in the visible portion of the spetrum and low dispersion. Two commonly used types of glass are

Fused Silica and Borosilicate. Fused Silica, more expensive, can stand high temperatures and starts softening around 1580C; the wafers are pure amorphous silicon dioxide (SiO_2). Borosilicate, most common is Pyrex, is similar to Fused Silica with a few exceptions such as its lower tolerance to heat, but its impurity non-uniformity makes precise etching difficult. Our process setups are discussed next.

Photolithography

Photolithography is the process of transferring geometric forms from a mask onto the surface of the substrate. Wafer cleaning, metallization, resist application, baking, alignment of the mask, exposure and development are an integral part of successful photolithography.

The wafers are first chemically cleaned to purify the surface from organic or metallic impurities. A second type of cleaning is needed after etching the substrate with plasma, which involves cleaning polymers that accumulate in the etching chamber during the process. The polymer cleaning is done using less aggressive oxygen plasma.

To clean the wafers from organics or metallic impurities the wafers were taken through the following steps:

1- 10 minutes in Sulfuric Acid: Hydrogen Peroxide bath (4:1 - 120ºC)

2- Thorough rinse in de-ionized (DI) water

3- 10 minutes in hydrochloric acid bath (5 H_2O: 1 H_2O_2: 1 HCl)

4- Thorough rinse in DI water

5- 30 seconds in hydrofluoric bath (50:1 at room temperature)

6- Final rinsing in DI water and drying

A thin layer of aluminum needed to be sputtered on the fused silica wafer for two main reasons. First, a reflective aluminum circle is located at the center of the device, as described in chapter two, which will stand for a mirror. Second, issues with the wafer-to-mask alignment in the projection stepper; the transparency of the substrate made it challenging for the machine to see the wafer and register to etched alignment marks. So a choice was made early to rely on metalized features that would stand for alignment marks. A layer 1000 Å thick of aluminum was sputtered on the wafer.

To define the alignment marks, resolution targets and verniers, an initial aluminum etch took place early in the process, so that it would be used as a foundation for subsequent alignments, and the different masks could register to it. The resist application, exposure and development will be detailed in the following sections in this chapter.

Etching the aluminum involved the following steps:

1- 30 seconds in DI water bath to wet the substrate surface
2- 30-40 seconds bath in an aluminum etchant (16 H_3PO_4 : 1 HNO_3 : 1 HAc : 2 H_2O – 50 ºC)
3- 10 minutes in DI water bath
4- Spin drying
5- 5 minutes in resist strip using PRX 127

The aluminum etching time varied slightly due to the small fluctuation (4 ^{o}C) of the temperature of the bath and also due to the decrease in purity of the etching solution after numerous etching cycles. The proposed resist stripping time was 20 minutes, however, this long exposure to PRX 127 roughened the metal traces and even attacked the substrate if left long enough in the bath. So the resist strip bath was decreased to 5 minutes only, which seemed not to cause any metal or substrate roughening.

Resist application

Photoresist is a radiation-sensitive polymeric material coating the substrate. It comes in two variants: negative and positive photoresist. For negative photoresists the UV-exposed regions are to be kept and not etched. UV light changes the chemical properties of the resist and becomes less soluble in developing solutions. When subjected to the developing solution the unexposed resist is simply washed away so that unprotected regions are left open to plasma exposure. The application of the photoresist is a critical step in the photolithography process as its uniformity affects the outcome of the etching directly. Spin Coating, high-speed centrifugal whirling, is the technique that is used to apply photoresist on the surface of the wafer.

The resist used in our process was Shipley 3612, which is a positive G/I line resist. To coat the fused silica wafer with 1.0 μm there was a need to first singe the wafer. Singe refers to heating the wafers to drive off any moisture on their surface. Right after the singe, an adhesion promoter, HexaMethylDiSilazane (HMDS) is applied to help the photoresist adhere to the surface of the wafer while it is resting on a hot plate, 125°C. Then a vacuum holder is spun at 5500 rpm for 30 seconds to yield a resist thickness of 1.0 μm, after which the wafer is baked on a hot plate at 115°C for 1 minute.

Masks, Alignment, and Exposure

A mask is a photodefinable chrome plated glass plate that contains the geometric shape that is to be imprinted on the photoresist by impinging photons onto the photoresist.

To design the different masks we have used L-edit Pro, which is a Tanner Research Inc. software. L-edit can be used to encode the phase contour data into a standard graphic format used by photomask-pattern generators called Graphic Design System II (GDS II). GDS II is simply a binary file used for transferring mask design from the designer to the mask fabrication facility, it is classified as data interchange format.

Mask 1 is a set on concentric rings with radii from 200 µm to 800 µm. From the center out to 200 µm it is a circle on top of which the metal layer will be laid. The smallest feature on mask 1 is 1.30 µm.

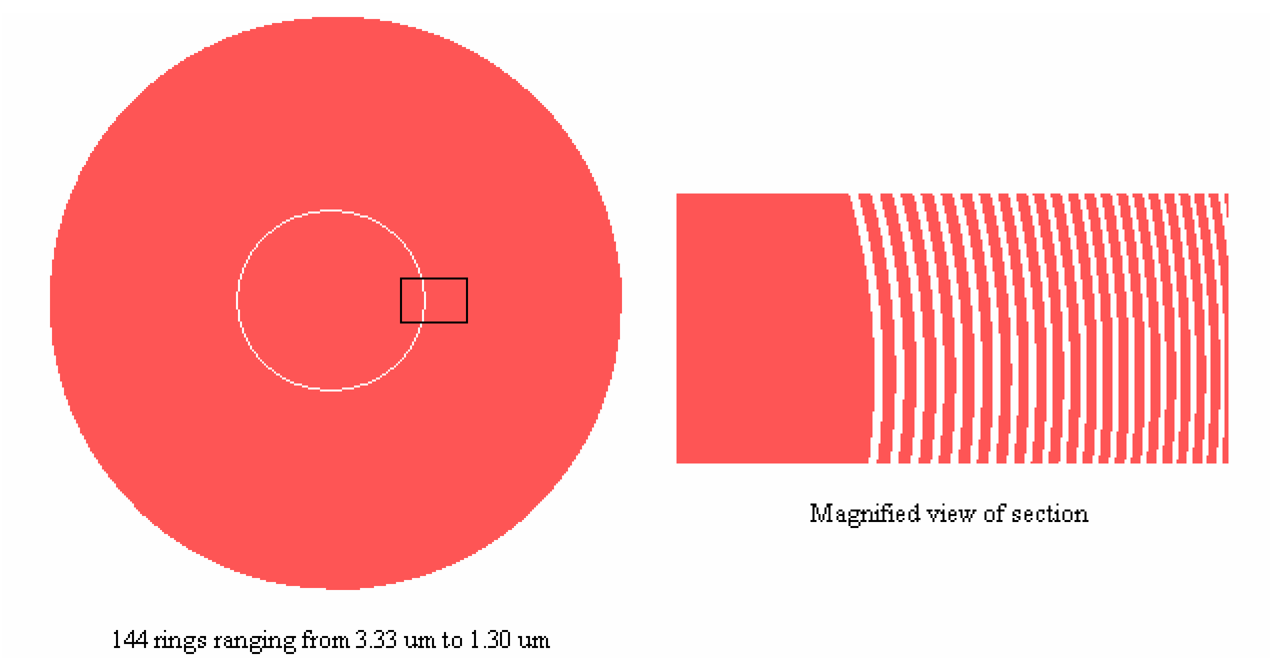

Figure 3.13: L-edit mask 1

Mask 2 is identical to mask 1 with twice the periodicity. Meaning if in mask 1 every 10.4 µm there were 8 rings in mask 2 there would only be 4 rings. The smallest feature on mask 2 is 2.60 µm.

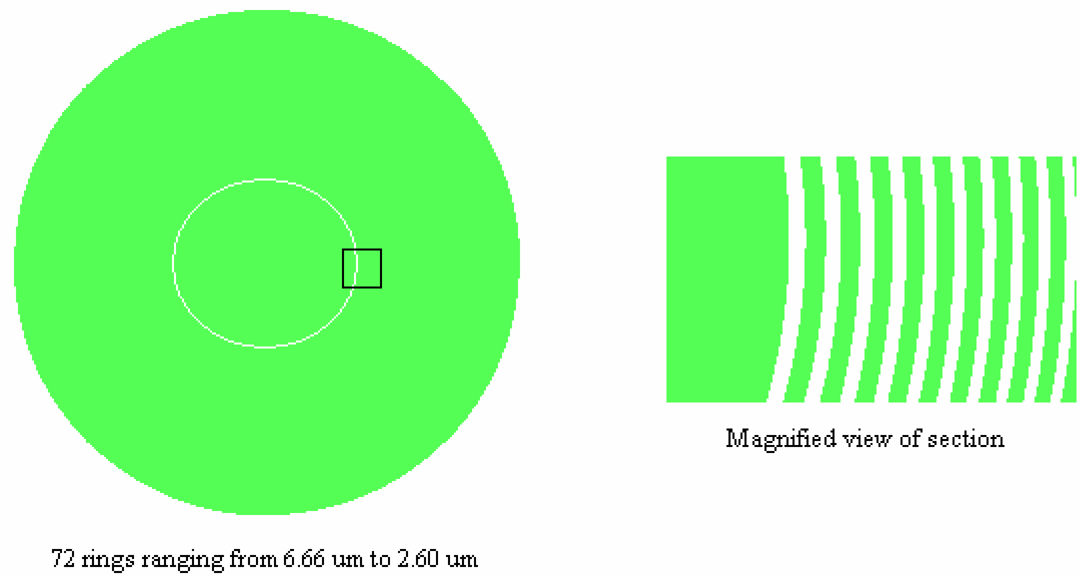

Figure 3.14: L-edit mask 2

Mask 3 had a smallest feature of 5.20 µm.

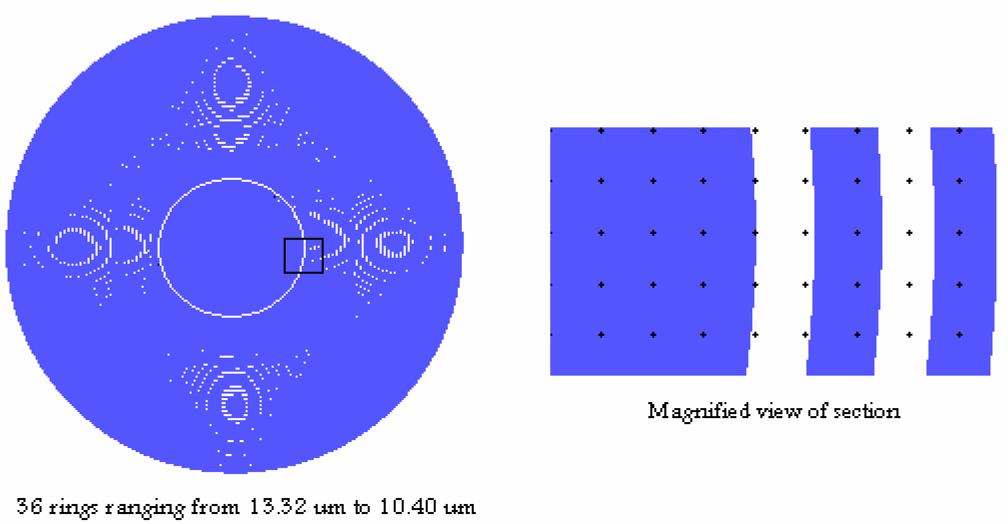

Figure 3.15: L-edit Mask 3

There was a need to have the masks made by a commercial vendor because of the abundance of curves in our design, the unfamiliarity of most CAD software with circular shapes made it difficult to produce in-house, SNF, masks that would reproduce curves with high fidelity.

The 5" masks used in our process were all made by COMPUGRAPHICS USA Inc., a company based in Los Gatos California. The smallest feature among all 4 masks was 1.3 μm. For the machine we were intending to use, a 5:1 projection stepper, the size on the mask was 6.5 μm.

Mask alignment is one of the most critical steps to the success of the entire photolithography. The mask is aligned with the wafer to allow the pattern to be transferred onto the wafer, and in successive steps each pattern needs to accurately register to the previous pattern with the highest accuracy. This becomes a challenging task with small feature sizes, highly symmetric shapes and increased number of masks. Once the mask has been accurately aligned to an existing pattern, the photoresist is exposed with a high intensity UV light.

Projection exposure is the best solution to achieve high resolution and sub-micron alignment accuracies as it allows for the mask to be, in the case of a 5 times projection, 5 times larger than the target pattern, then the image is de-magnified and projected onto the photoresist. The reduced image is stepped over a selected surface of the wafer. The reduction stepper is capable of 1.0 μm resolution or lower.

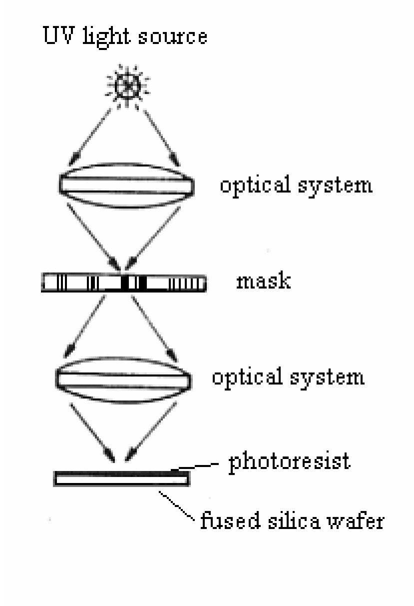

Figure 3.16: Reducing projection

For exposure, we used the Nikon NSR, repeat and reduction stepper. The Nikon NSR offers a field of exposure of 15 x 15 mm, alignment accuracies in the 0.18-0.25 μm range, and an impressive 0.6 μm resolution as proven by the SEM taken by members of the staff at SNF.

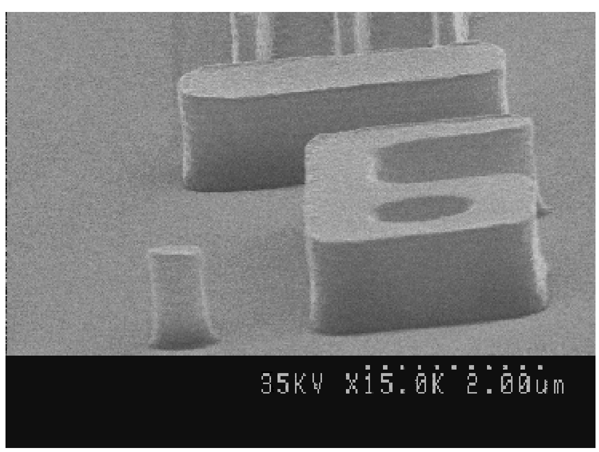

Figure 3.17: Resolution mask with Shipley 3612

Optical lithography results were reasonable for our needs, resorting to e-beam lithography would have been a luxury, especially that our design consists of curved shapes which will take an extensive amount of time on an e-beam writer.

After exposure, the photoresist is developed so that the weak regions are washed away, unexposed regions if using negative photoresist and exposed regions for positive photoresist. Photoresist constitutes itself a mask that will be used in the next step of etching. The developing solution we used was LDD26W in which the photoresist was developed for 60 second then baked on a115 °C hot plate. The resolution was checked immediately after development and was measured to be 0.60 µm.

Etching

There are many techniques used for etching, all of which can be categorized either under wet chemical etching or dry etching. Wet chemical etching is mainly isotropic, material removed equally in all directions. Whereas dry etching is anisotropic and thus offers considerable profile control and flexibility, that is why it is the primary method of pattern transfer that is used in binary optics technology. To fabricate our device we have used plasma etching so we will limit ourselves to discuss plasma processes and physics. It is important to understand the different plasma processes and its physics in micro-optics applications where the slightest deviation, registration or depth accuracy, in the fabrication will result in lower optical efficiencies.

Plasma etching is a key technology when optical structures are transferred onto the photoresist, to an underlying material, in our case fused silica. The main application for plasma etching is the fabrication of nanometer-sized structures in different materials for state of the art integrated circuits.

Figure 3.18 shows the steps involved in photoresist layout, aluminum sputtering and etching the substrate (fused silica), as well as the thickness of the aluminum layer and the photoresist.

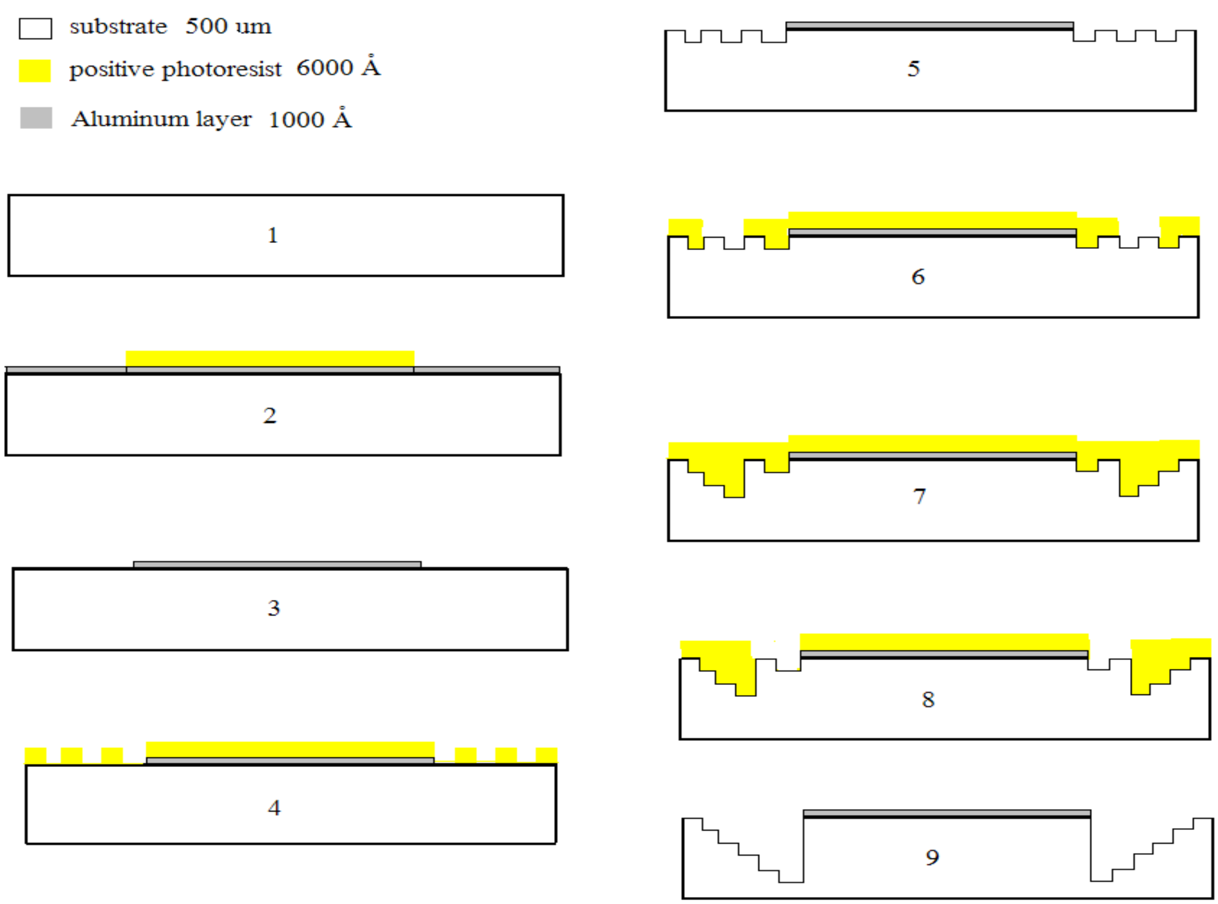

Figure 3.18: Photoresist, aluminum layout for the formation of the 8-step profile micromachining

Plasma background information

To etch the fused silica wafers we have used the AMT 8100 etcher, which is a reactive ion etcher for oxides and nitrides. Before going into the etcher the wafers had to

be UV-baked for 15 minutes and put in a 110°C oven for 1 hour in order to avoid resist burning. The AMT etcher is a fluorine based chemistry etcher, which fitted our goals as we had a choice between using CF_4 or CHF_3. After a few trials with CF_4 and after consulting with Dr. Don O'Shea of Georgia Tech and Dr. Tom Suleski of DIGITAL OPTICS Corp., we decided to use CHF_3. The main reason for such a decision was that CF_4 is more aggressive on fused silica and roughens it. So after seasoning the empty chamber for 15 minutes, we run etch tests that yielded and average etch rate of 330 Å/minute, which was close to the specifications of the machine of 354 Å/minute.
The recipe used was that of Via Etch. The pressure in the chamber was 50 mTorr. O_2 flow was 30 sccm in the chamber, while CHF_3 was 50 sccm with no particular setting for temperature (room temperature), the RF power was left unchanged at 1400 W.

Etch duration	240 sec	480 sec	960 sec
Target depth	135 nm	270 nm	540 nm
Measured depth-center of device	123 nm	267 nm	562 nm
Measured depth-edge of device	127 nm	268 nm	560 nm
Percent error-center of device	8.88 %	1.11 %	4.07 %
Percent error-edge of device	5.92 %	0.74 %	3.70 %

Table 3.2: Fused silica etch depth measurements on the AMT 8100

As can be seen from table 3.2 the measured depths are all very close to the target depths. The measurements were done on two devices, one located at the center of the wafer and the second on a device located towards the edges of the wafer. There was no noticeable difference between the etch depths and lateral dimensions at the two locations of the wafer.

Fabrication Results

Throughout the process, we were able to make tests to support our predictions of how accurately we would be able to approach the previously mentioned relief depths. The first test concerned a 2-level profile. An image acquired using an Atomic Force Microscope (AFM) gave the following results

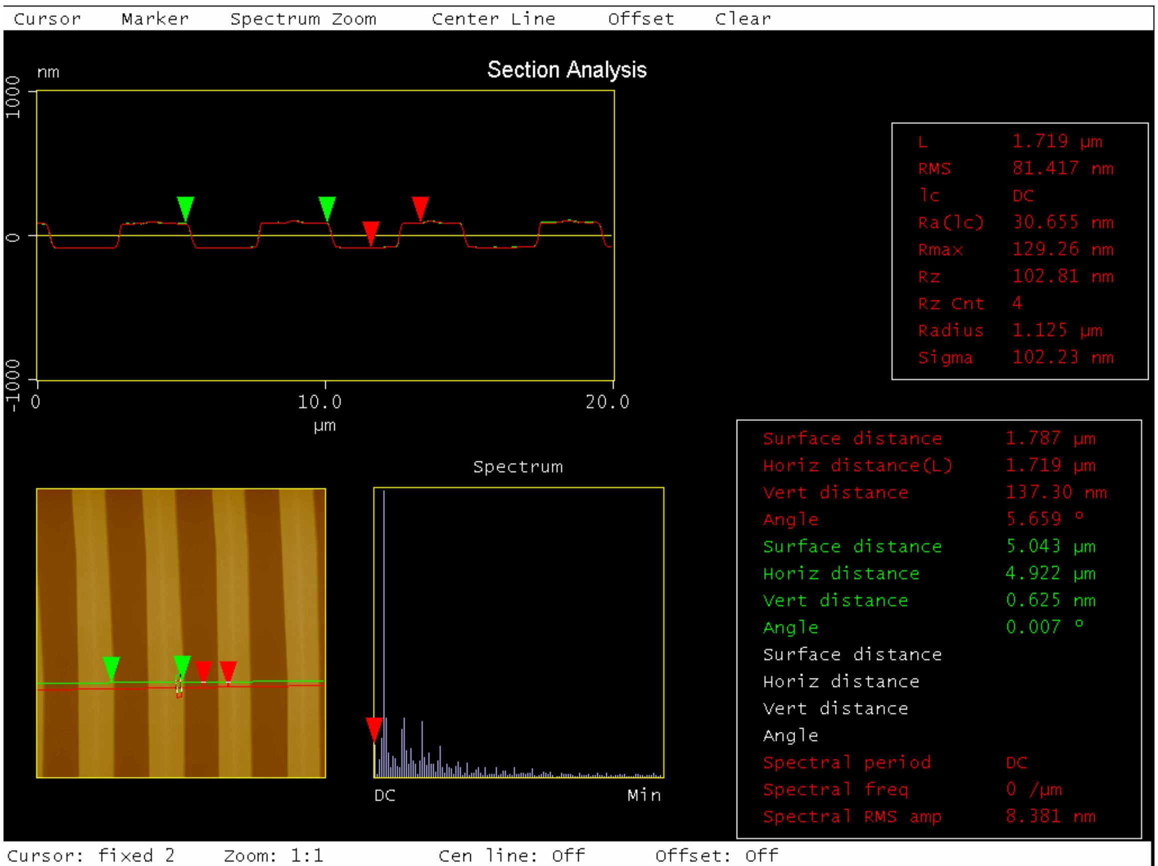

Figure 3.19: AFM image of 2-level profile

From the reading of the AFM in figure 3.19, one can see that the step depth is 137.3 nm, which is 1.7% off from the 135 nm target. As a means of judging how well leveled the different steps are, the difference between two leveled steps was measured to be 0.625 nm. Figure 3.20 is a side view of the etched device

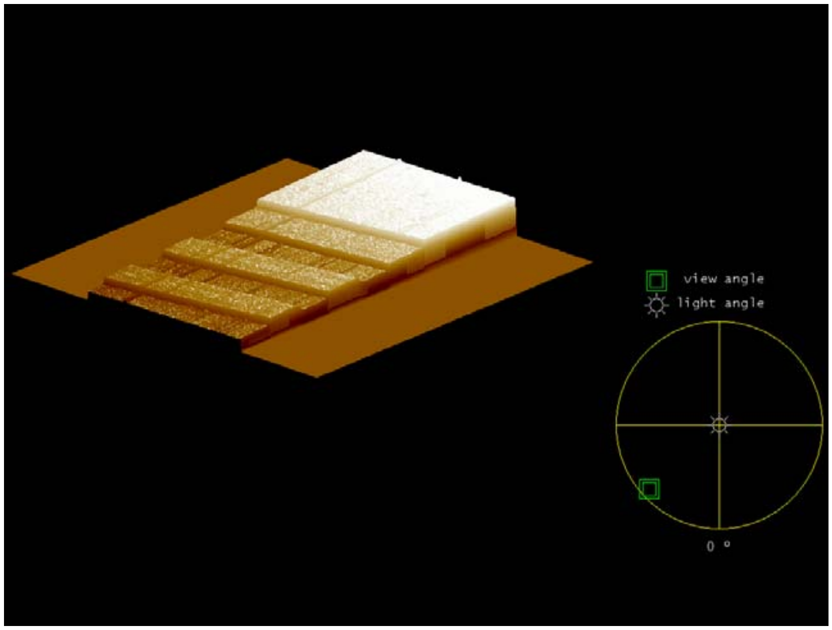

Figure 3.20: AFM side-view of 2-level profile

The AFM in figure 3.21 and figure 3.22 show how the 4-step phase profile is nicely defined and that the vertical distance between two steps is 273.03 nm while the target depth is 270 nm, which is only 1.12 % off. One can also notice the sloping of the sidewalls. The reason for the sloping could be in the photolithographic process or could simply be due to the AFM imaging its own tip instead of the side of the profile as can be seen later in figure 3.23.

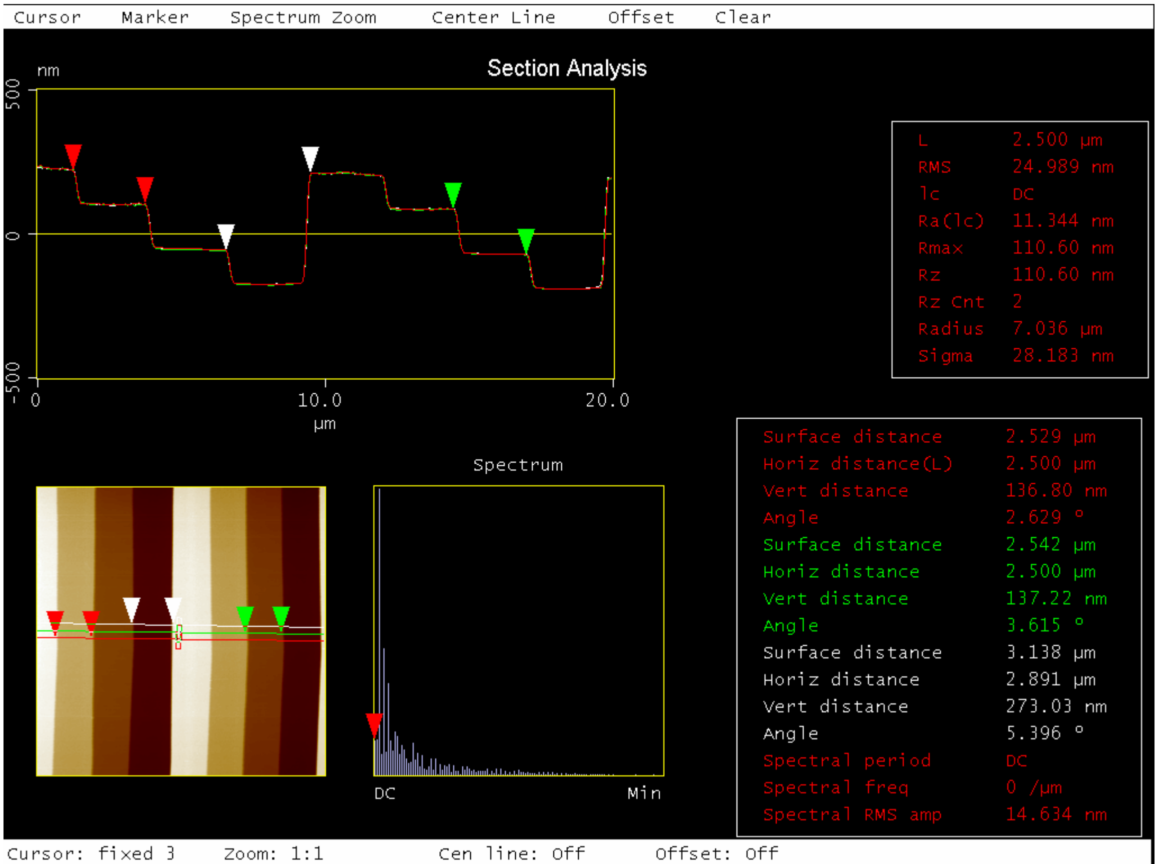

Figure 3.21: AFM image of 4-level profile

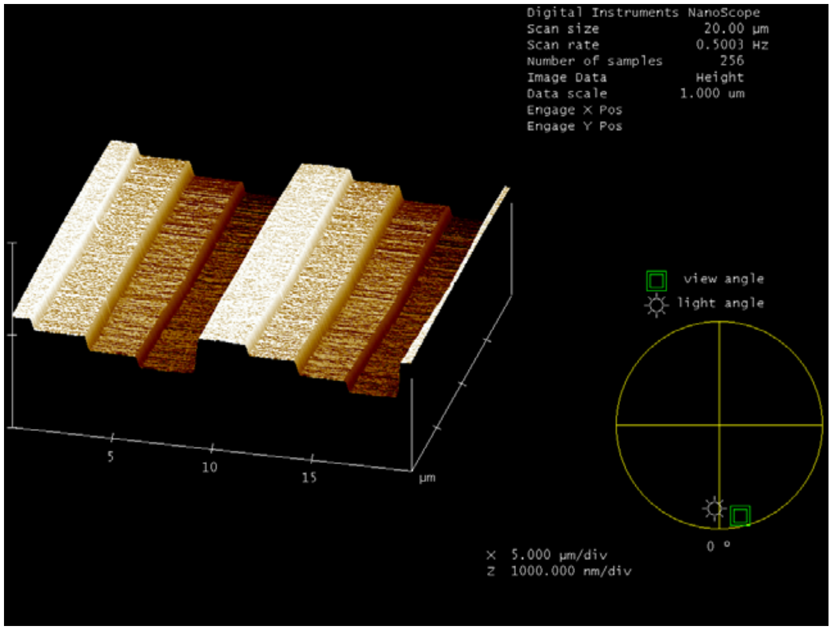

Figure 3.22: Side-view of 4-level profile

The side view in figure 3.22 gives proof of near-perfect pattern registration as there are no trenches or ridges and the profile is the predicted staircase at the second etch phase.

The last step was to align, expose then etch one last time to finalize the 8-step profile. The last mask has the largest features of all masks, still accurate alignment is critical to take the fabricated DOE from a theoretical diffraction efficiency of 81% to 95%.

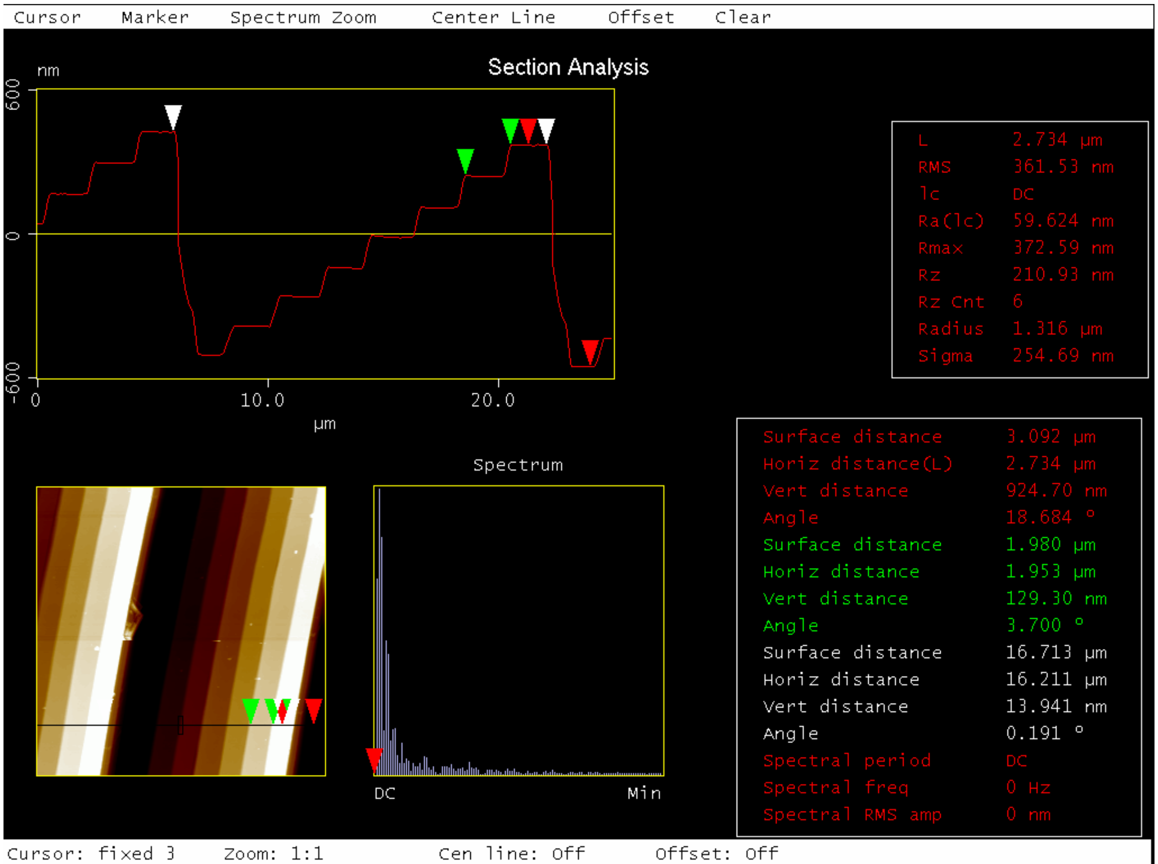

Figure 3.23: AFM image of 4-level profile

As can be seen from the AFM image in figure 3.23, there are 8 distinct steps, without trenches or ridges, which implies that the alignment of the third mask was done very accurately. There is an expected sloping to the sidewalls, which seems to be flat in the upper portion of the sidewall and has a little slope to it towards the bottom. The sloping towards the bottom is most likely due to the AFM tip, which was imaged instead of the contour of the actual device.

Figure 3.24 shows a side view of two periods of the DOE with well defined steps. An SEM of the DOE is shown after being diced into a hexagon in figure 3.25.

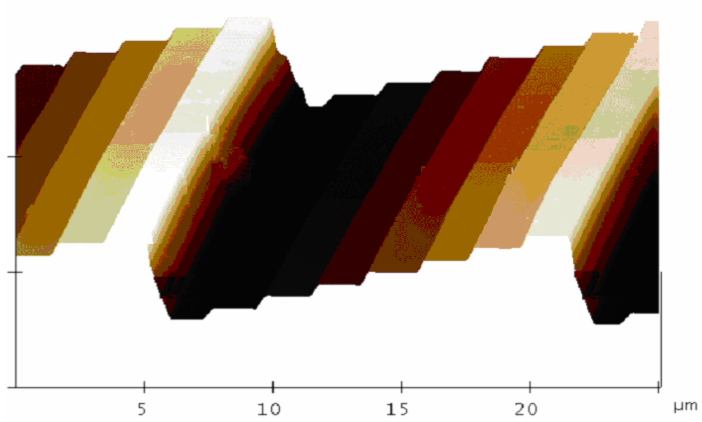

Figure 3.24 Side-view of 8-level profile

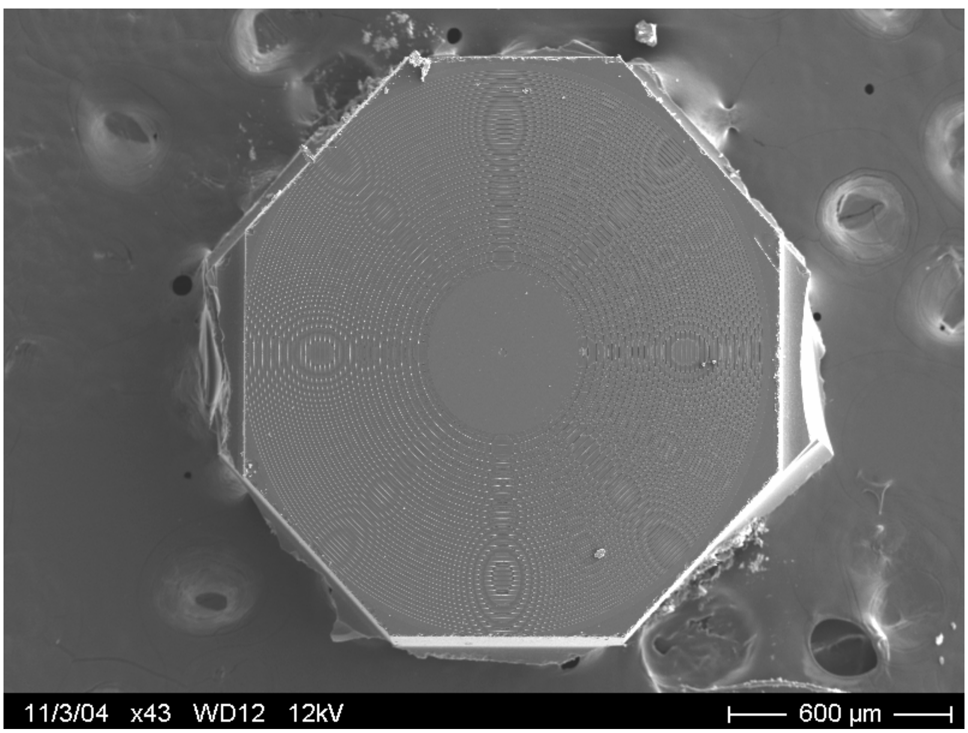

Figure 3.25: SEM of an 8-level DOE

Diffraction Efficiency Measurement

First order diffraction efficiency tests were made by taking light to a slow focus onto the DOE. Light was collimated through a long focal length lens (50.0 cm), in order to confine the beam to a portion of the DOE. The power of the first order diffracted light was measured and compared it to the power of un-diffracted light going through the same fused silica thickness, 500 μm.

Measurement tests were made to compare how closely the fabricated DOE matched the theoretical data. Measurements were taken at discrete different wavelengths, 457 nm, 472 nm, 488 nm, 496 nm, 502 nm, and 515 nm.

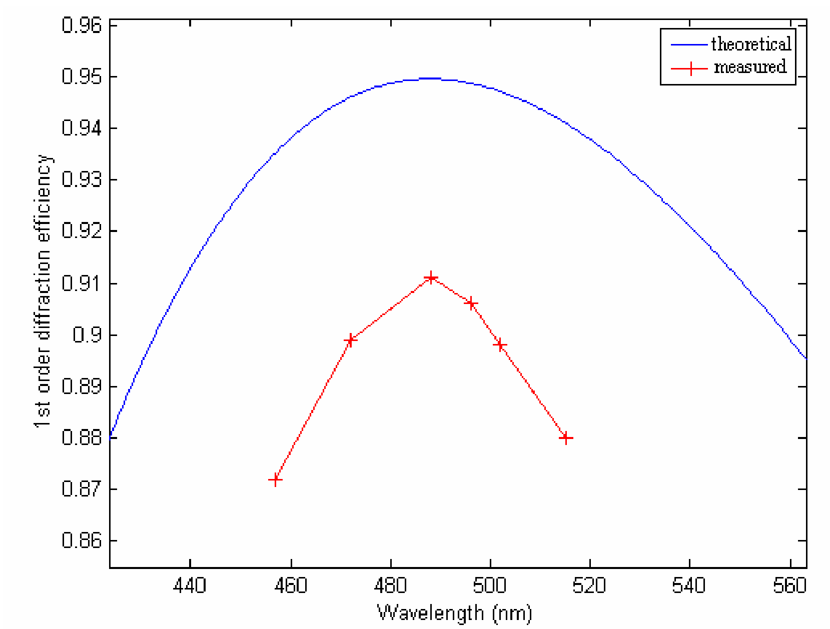

Figure 3.26 Theoretical vs. measured 1st order diffraction efficiencies

In figure 3.26, it can be seen that the measured results graph shows lower diffraction efficiency values but follows the same pattern as the theoretical results graph. The optimum measured 1st order diffraction efficiency occurring at 488 nm is 91% for an expected value of 95%, and at 515 nm it is 88% for an expected value of 94% according to equation 3.3. The difference is expected due to the minimal errors associated with the microfabrication such as surface relief depth tolerance the targeted etch depths were less than 3% off from the expected values, and possible misalignment could also be a reason for lower diffraction efficiency.

CHAPTER FOUR

EXPERIMENTAL LENS CHARACTERIZATION

Objective Lens Performance

The objective lens gave very satisfactory simulation results as the point spread function, lateral chromatic and spherical aberrations were minimized.

Optical Path Difference (OPD), which is the difference between the two optical path lengths of the target wavelengths, was calculated for different configurations. On-axis maximum scale was 0.200 waves, and 1.000 waves off-axis.

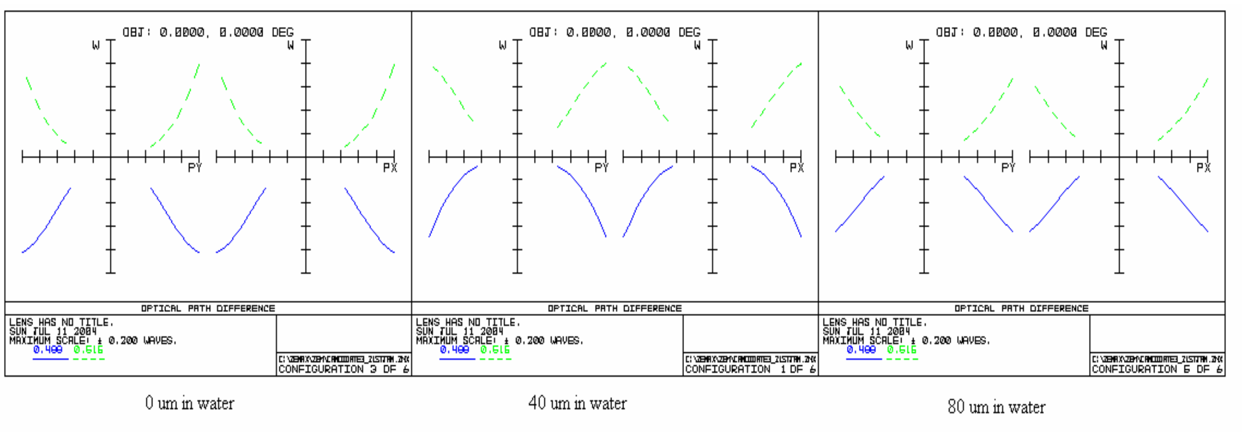

Figure 4.1: On-axis optical path difference

The on-axis OPD shows some longitudinal spherical aberration that does not exceed 0.200 wave and chromatic aberrations which appear to be dominant.

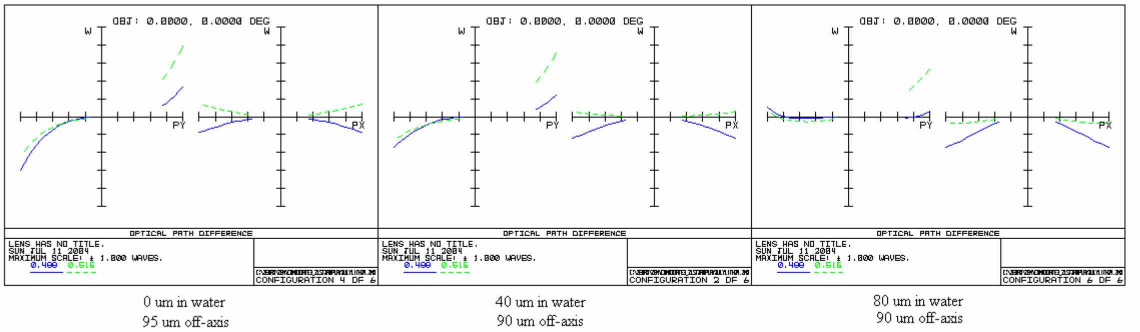

Figure 4.2: Off-axis optical path difference

From the shape of the graph one can see some spherical aberration on the on-axis plot, and a little coma on the off-axis plot. The effect of these aberrations will be even further decreased because of the use of the MEMS scanning deformable mirror, which will further decrease their effects.

The precision in lateral discrimination depends on the Point Spread Function (PSF). Consider an object whose size is one single point, we think of its image to be at least one pixel large. However, if looked at carefully it will be several pixels, with the brightest pixels at the center while the pixels around it gradually become dimmer; this image function is what is called a PSF. The more concentrated the pixels the higher the resolution. The resolution will be defined as the width of the PSF when it reaches half its maximum value, commonly called Full Width at Half Maximum (FWHM).

Based on Zemax simulations the PSF was measured at different locations. The FWHM was measured to reach a minimum of 0.680 µm at 488 nm, and 0.700 µm at 515 nm.

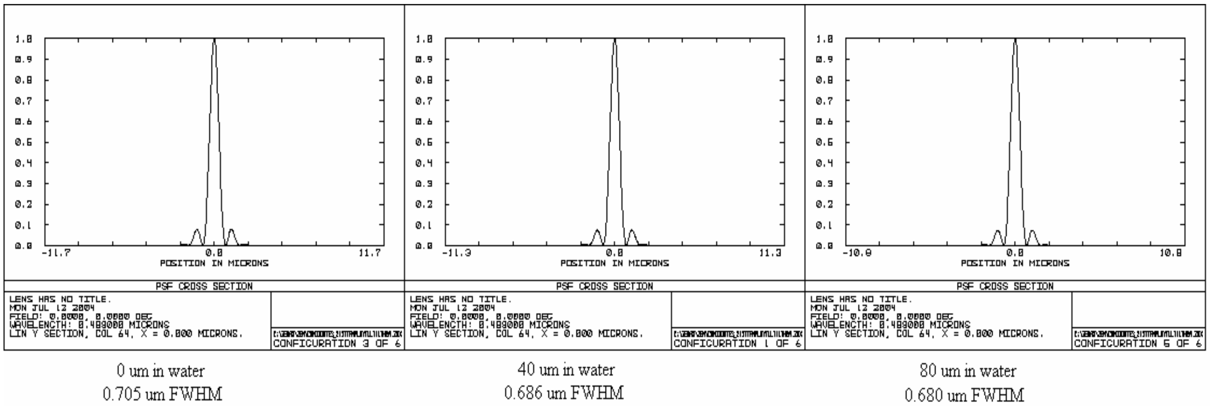

Figure 4.3: Simulated normalized on-axis PSF at 488 nm

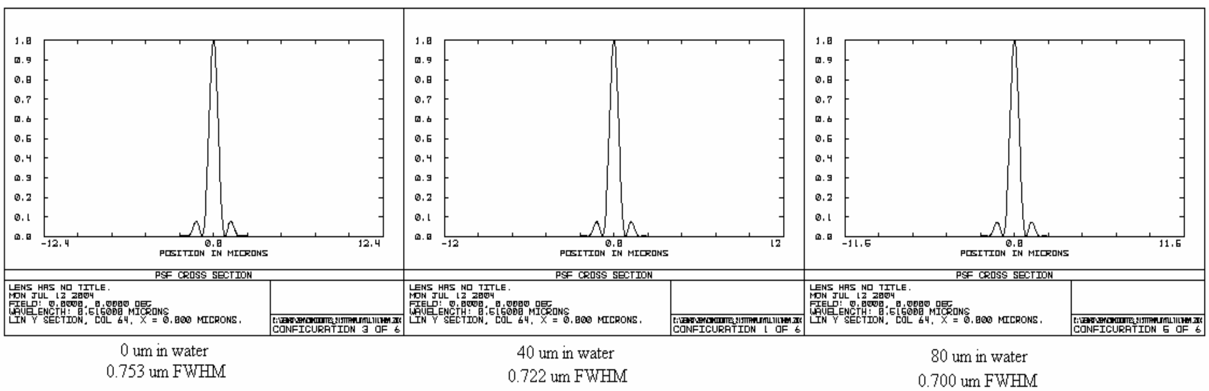

Figure 4.4: Simulated normalized on-axis PSF at 515 nm.

Figure 4.5 shows the spot size at 488 nm and 515 nm wavelengths at different foci inside water.

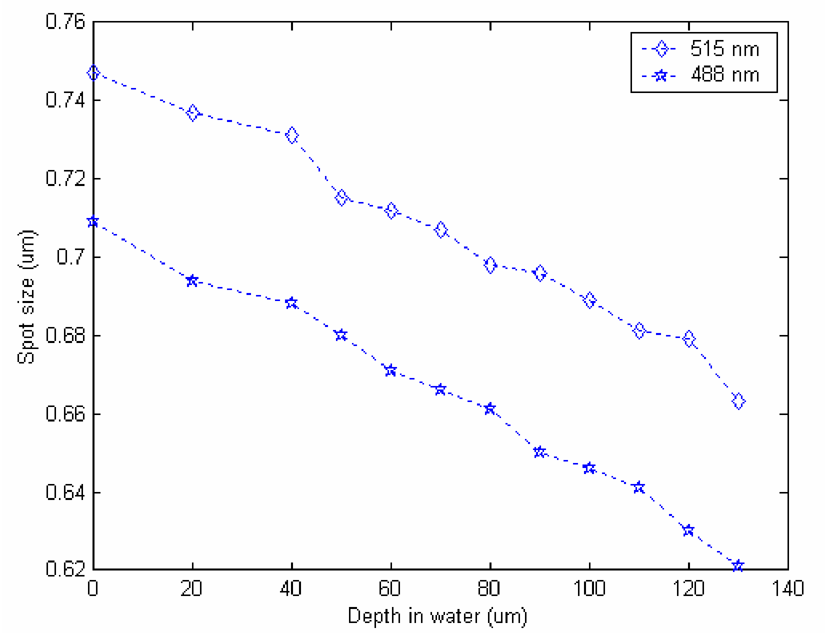

Figure 4.5: On-axis PSF change inside water (Zemax results)

The spot sizes for different foci at 488 nm appear to be smaller than those at 515 nm. In fact, the spot sizes should almost be identical, but the data were taken in such a way that the image plane was placed first where the 488 nm focus occurred and the FWHM was recorded, and without moving the image plane the FWHM was measured at 515 nm. Due to longitudinal color, the two different wavelengths focused at different places; that is where the slight increase in spot size for 515 nm occurred. The measurement itself was done by taking the image plane and measuring the minimum spot size at 488 nm and without the location of the image plane measuring the spot size at 515 nm which might have also introduced the difference in spot size.

Beyond 130 μm deep inside water, the deformable mirror is low power, so mostly flat, the decision was taken to limit ourselves to this depth.

The PSF was analyzed off-axis as well, figure 4.6 and figure 4.7 below show some sample points at 488 nm and 515 nm. The PSF off-axis was measured at 90 μm off-axis.

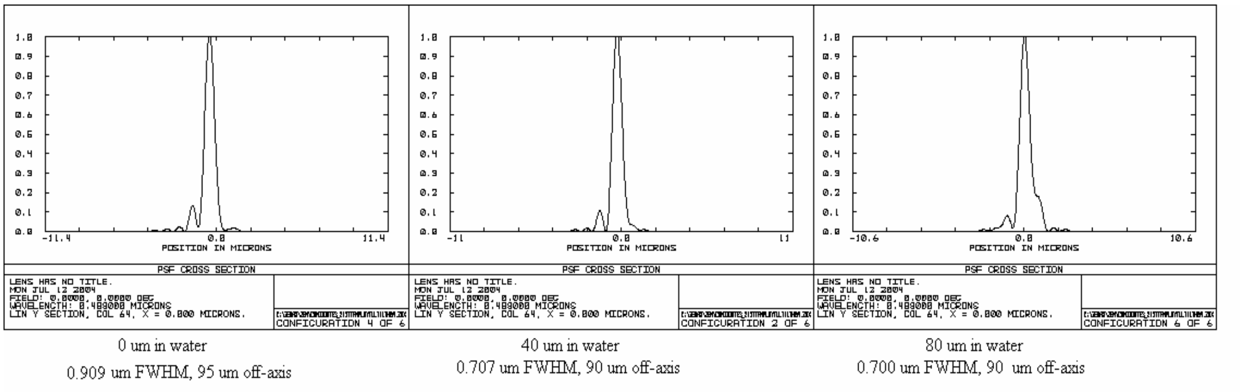

Figure 4.6: Normalized PSF off-axis at 488nm (Zemax results)

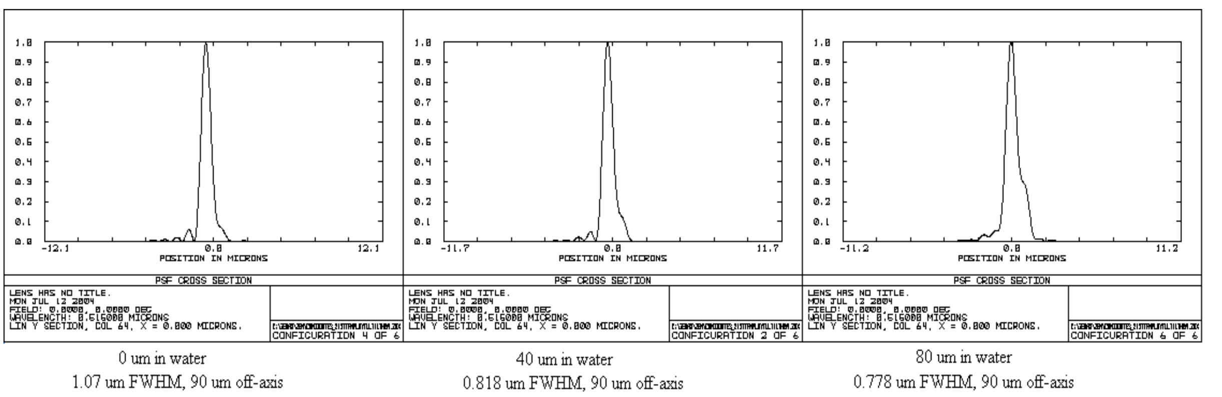

Figure 4.7: Normalized PSF off-axis at 515nm (Zemax results)

Plots in 4.6 and 4.7 are slices through the asymmetric plane of the PSF. The axis 90 degrees from these slices were symmetric. The asymmetry is evidence of coma. For off-axis FWHM the same data taking process was followed, so spot size decreases until it reaches a minimum at 70 μm deep inside water, then starts increasing past this depth as figure 4.8 shows.

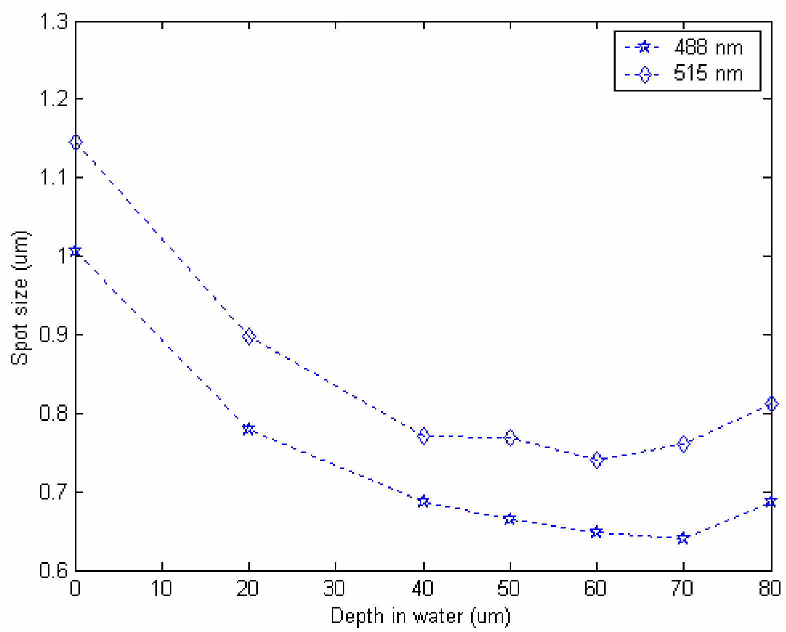

Figure 4.8: Off-axis PSF change inside water (Zemax results)

Experimental Characterization

The objective lens was packaged and set up to be able to take measurements to compare the results obtained using Zemax with the actual performance of the 3 refractive lenses and the DOE described in chapter three. On an optical table, an Argon Ion laser operating in the 450 nm to 515nm range was used as a light source. A singlemode 488 nm optical fiber was stripped at its end and introduced inside the fused silica tube. At this stage the deformable mirror was not introduced. In the Zemax simulation with the deformable mirror, light traveled about 4.00 mm before reaching the DOE, so in the experiment the optical fiber was pulled 4.00 mm back to simulate a similar effect. An infinity corrected immersion lens was introduced (Nikon CFM Plan APO 20X, 0.75 NA and 0.35 mm working distance), and different long focal length lenses (0.300 m, 0.500 m, and 1.00 m) to focus the beam and obtain the desired magnification.

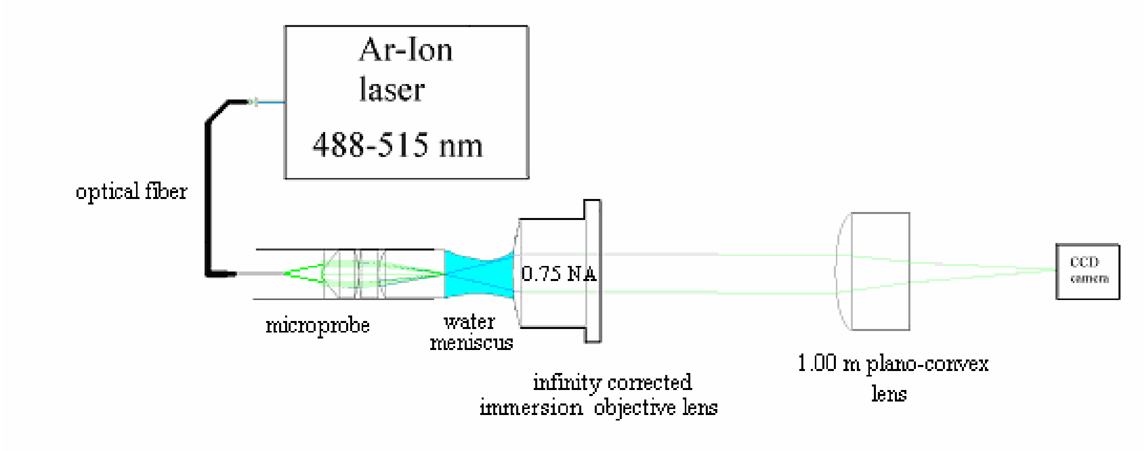

Figure 4.9: Experimental setup used for testing the objective lens

Experimental Results

On-Axis Performance

The results taken on-axis were similar in their pattern to the simulation, meaning the deeper we imaged in water the smaller was the FWHM. The smallest measured spot size was 0.703 µm.

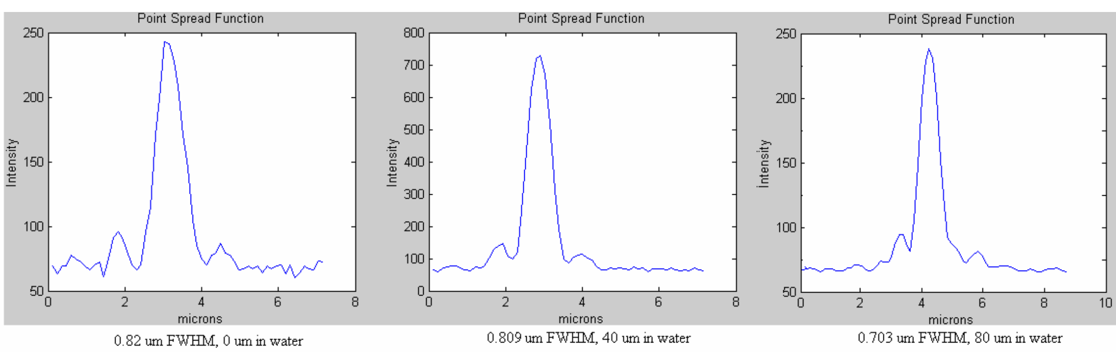

Figure 4.10: Measured on-axis PSF at 488 nm

For non-confocal settings $R_{lat} = \frac{(0.5\lambda)}{NA}$ (2.1) the spot size should reach a minimum of 0.680 μm, which is 3.3% away from the measured value of 0.703 μm. There is a small asymmetry in the PSF, which could be due to a lens being tilted in the probe.

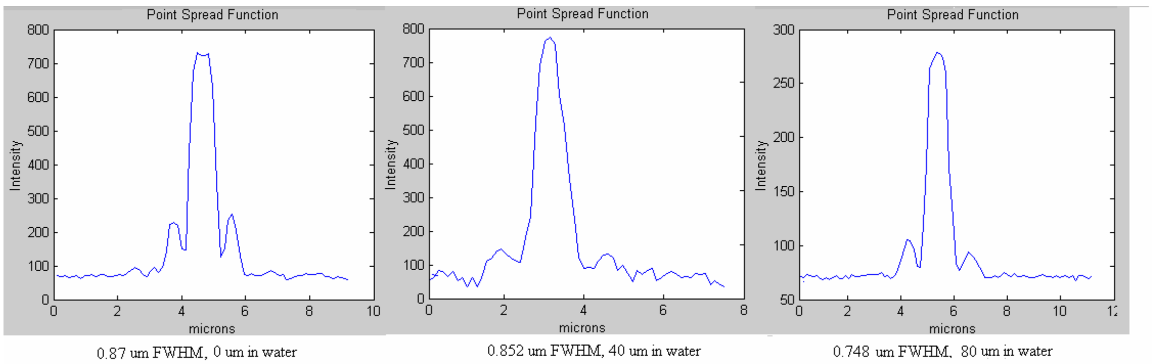

Figure 4.11: Measured on-axis PSF at 515 nm

In the instance of the PSF at 515 nm, the minimal spot size occurred deeper in water at 90 μm, where the spot size was 0.735 μm, less than 3% off from the expected value of 0.717 μm at 80 μm in water.

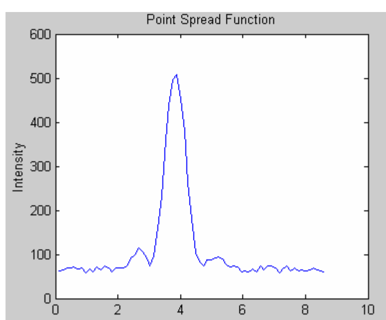

Figure 4.12: On-axis FWHM of 0.735 μm at 515 nm 90 μm deep in water.

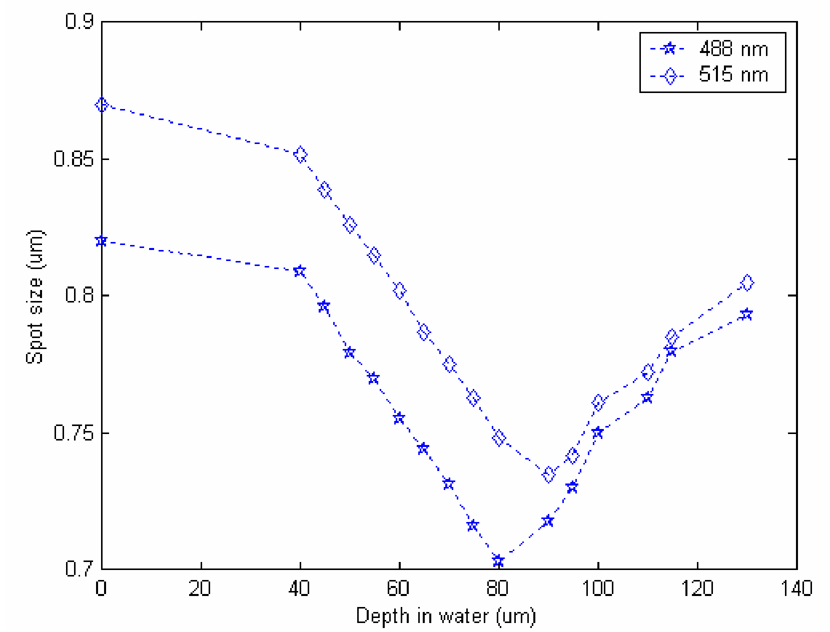

Figure 4.13: Measured on-axis PSF change inside water

Off-Axis Performance

Three different lenses were used (0.300 m, 0.500 m, and 1.00 m) to be able to measure the PSF away from the optical axis. We have measured the PSF at multiple points and figure 4.14 and figure 4.15 show the PSF 60 µm off-axis.

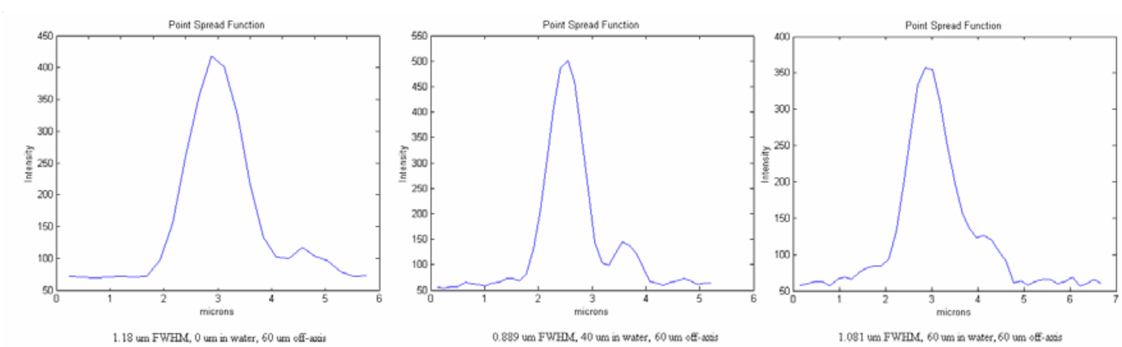

Figure 4.14: Measured off-axis PSF at 488 nm at different locations 60 µm off-axis.

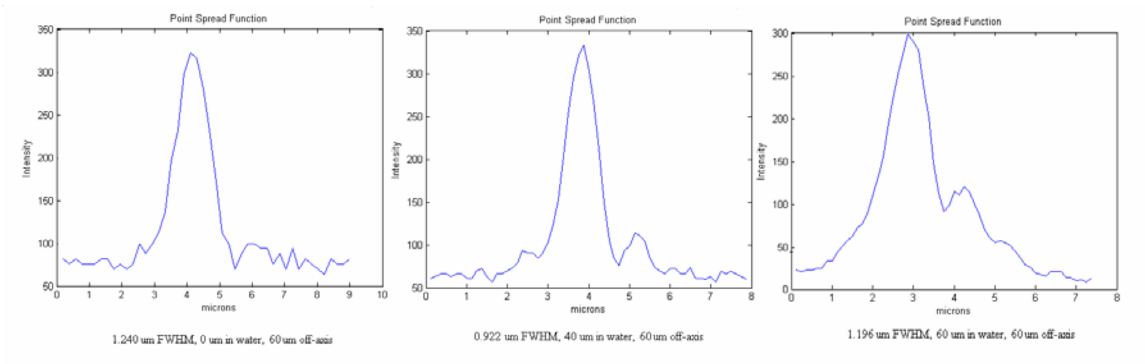

Figure 4.15: Measured off-axis PSF at 515 nm at different locations 60 µm off-axis.

The plots off-axis show some significant coma. In the Zemax simulation, the off-axis spot size at 488 nm is expected to be minimal 70 µm inside water with a FWHM of 0.700 µm and 0.778 µm at 515 nm.

Experimentally the best off-axis focus occurs at a shorter depth, 40 µm, with a larger FWHM, 10 % to 20 % larger.

Conclusions

The ray tracing software simulation predicted closely the behavior of the optical system on-axis as shown in the experimental results with sub-micron spot sizes as deep as 140 µm in water for both wavelengths with only 3% error difference. Off-axis, the experimental results were not as closely matched to the ray tracing simulations, 10% to 20 % error difference.

The relatively large off-axis error might be caused by a number of factors, among which are assembly and alignment errors, DOE defect, or fiber optic tip bending.

Assembling the refractive lenses and the diffractive optical element was a tedious task, which was successfully accomplished. High accuracy stages were used to perfectly align the DOE with the lens it was glued on top of, using a UV-curable epoxy suitable for optical applications. The lenses were carefully then inserted in the tubing and pushed against each other. The end of the tube was finally sealed using UV-curable epoxy to eliminate any space between the lens and the inner wall of the tube. More automated means for mounting, aligning and inserting lenses could ensure perfect packaging and more confidence in isolating the reasons for potential discrepancies with simulations. A means to handle the small lenses (1.6mm in diameter and 0.65 mm thick) safely without risking scratching or breaking them would an excellent asset to ease the handling and the assembly of the lenses.

CHAPTER FIVE

CONCLUSIONS

In conclusion, the design, the fabrication, and the testing of the micro-objective lens have been successful. Lens dimensions are 4.0 mm in length and 2.0 mm in diameter. The actual optics size excluding the packaging, tubing to hold the lens and the fiber, was 4.0 mm in length and 1.6 mm in diameter.

Zemax ray tracing software was also used to determine, lens thickness, radii of curvature, and DOE phase function to minimize chromatic and spherical aberrations, coma to achieve minimum wavefront aberration and PSF. The full width at half maximum (FWHM) was minimized for both design wavelengths. On-axis FWHM was measured in the finished lens to be 0.70 μm at 488 nm and 0.74 μm at 515 nm, with a percentage error compared to simulations of less than 4%. Off-axis FWHM was measured to be 0. 90 μm at 488 nm and 0.92 μm at 515 nm 40 μm deep and 60 μm off-axis in water. Off-axis results were worse than predicted by the simulation, 25% off at 488 nm and 15% off at 515 nm. The discrepancy could be due to imperfect lens alignment in the tubing and lens tilting. The results should get better when the MEMS scanning deformable mirror will be made to work properly, as its main advantage, besides scanning, is to further reduce spherical aberrations.

The design of the diffractive optical element started from the phase function suggested by the ray tracing software. The phase function equation was translated into step profile by choosing the number of steps desired in the profile, thus the depth and width of each step. As for the fabrication of the DOE, the masks designed with L-edit, which were successfully aligned and superposed on each other, exhibited almost no issues related with misalignment. The measured resolution after developing the photoresist was witnessed to be 0.6 µm, which is considered satisfying for photolithography. If there was a need for a higher exposure and etching quality, one can resort to e-beam lithography, the resolution is far higher, however due to the curved nature of the design it will be considerably expensive and time consuming.

The choice to start with ball lens values to make the plano-convex lenses was a good choice because choosing other radii than standard radii available with ball lenses is considerably more expensive. From a lens manufacturer perspective, it is simpler to start with a ball lens and grind it into a plano-convex lens rather than starting with bulk glass. Investigating possibilities to make negative lenses would be beneficial to decrease aberrations further and obtain a similar performance with fewer lenses. Use of negative lens elements would offer the possibility of correcting chromatic aberrations without the use of a DOE.

Having to insert the lens into the tube was done under the assumption that the alignment would have been near perfect, however diameter tolerances of both the tube and the lens allow for tilting of the lenses inside the tube, which worsens the optical performance. To perfectly align the lenses, they could be assembled on a holder and covered with epoxy. One issue that could be encountered is that epoxy wicks between the lenses, that is why a transparent film could be used to cover the lens set before applying the epoxy. This approach would also avoid scratching the lenses while inserting them in the tubing.

REFERENCES CITED

[1] K. Carlsson, P. E. Danielsson, R. Lenz, A. Liljeborg, A. Majlof, N. Aslund, "Three-Dimensional Microscopy Using a Confocal Laser Scanning Microscope," Optics Letters 10, 53-55, 1985.

[2] P. Wallen, K. Carlsson, K. Mossberg, "Confocal Laser Scanning Microscopy as a Tool for Studying the 3-Morphology of Nerve Cells," Visualization in Biomedical Microscopes. 3-D Imaging and Computer Applications, chapter 5, Editor: A. Kriete, VCH Verlagsgesselschaft mbH, Weinheim, 1992.

[3] M. Minsky, "Memoir on Inventing the Confocal Scanning Microscope," Scanning Vol 10, No. 4, 128-38, 1988.

[4] L. Majlof, P. O. Forsgren, "Confocal Microscopy: Important Considerations for Accurate Imaging," Methods in Cell Biology, Vol 38, 79-95, Editor: B. Matsumoto, Academic Press, 1993.

[5] T. R. Corle, G. S. Kino, "Confocal Scanning Optical Microscopy and Related Imaging Systems." Academic Press, London, 1996.

[6] M. Gu and C.J.R. Sheppard, "Three-dimensional optical transfer function in the fibre-optical confocal scanning microscope using annular lenses." J. Opt. Soc. Amer. A., 9, 1991-1999, 1992.

[7] M. Gu, X. Gan, C.J.R. Sheppard,"Three-dimensional coherent transfer functions in fibre optical confocal scanning microscopes." J. Opt. Soc. Amer. A., 8, 1019-1025, 1991.

[8] W. J. Smith, "Modern Optical Engineering," McGraw Hill, 1990.

[9] K. Sauermann, S. Clemann , S. Jasper "Age related changes of human skin investigated with histometric measurements by confocal laser scanning microscopy in vivo." Skin Res Technol 2002;Vol. 8, 52-56

[10] H. P. Herzig, "Micro-Optics: Elements, Systems and Applications," Taylor & Francis, London, 1997.

[11] E. Hecht, "Optics," Addison Wesley, 2001.

[12] G. J. Swanson, "Binary optics technology: theoretical limits on the diffraction efficiency of multilevel diffractive optical elements," Technology Report Lincoln Laboratory, Massachusetts Institute of Technology, 1991.

[13] W. B. Veldkamp, G. J. Swanson, "Development in Fabrication of Binary Optical Elements ," Proc. SPIE 437, 54, 1983.

[14] Y. Ogura, N. Shirai, J. Tanida, and Y. Ichioka, “Wavelength-multiplexing diffractive phase elements: design, fabrication, and performance evaluation,” J. Opt. Soc. Am. A. Vol 18, 1082 – 1092, 2001.

APPENDIX A

ZEMAX Merit Function

The merit function presented in this appendix has been modified from the default merit function in Zemax-EE version 10.0.

Operands were added during the design process to limit the physical dimensions of the optical systems such as maximum center thickness glass (MXCG), maximum curvature (MXCV), maximum edge thickness glass (MXEG), and total thickness less than (TTLT). Other operands to minimize aberrations were lateral color (LACL), axial color (AXCL), and spherical aberration (SPHA).

The merit function outlines four configurations. In the first configuration, the focus is on the last surface of the objective lens (L3) on-axis, while it is off-axis in configuration 2. Configurations three and four are optimized respectively on and off-axis at a depth of 100 µm. In the four configurations the optimization takes place for the two different wavelengths, 488 nm and 515 nm.

#	Type	Int1	Int2	Px	Py	Target	Weight	Value	Contrib
1	CONF	1	0	0.00E+00	0.00E+00	0.00E+00	0.00E+00	0.00E+00	0.00E+00
2	LACL	0	0	0.00E+00	0.00E+00	0.00E+00	5.00E+05	0.00E+00	0.00E+00
3	SPHA	1	1	0.00E+00	0.00E+00	0.00E+00	5.00E+05	-1.56E-03	1.15E-01
4	SPHA	1	2	0.00E+00	0.00E+00	0.00E+00	5.00E+05	-1.50E-03	1.10E-01
5	EFFL	0	1	0.00E+00	0.00E+00	1.00E+00	5.00E+05	1.21E+00	1.56E+01
6	EFFL	0	2	0.00E+00	0.00E+00	1.00E+00	5.00E+05	1.21E+00	1.50E+01
7	AXCL	0	0	0.00E+00	0.00E+00	0.00E+00	5.00E+07	-1.66E-03	9.76E-02
8	MCOL	2	1	0.00E+00	0.00E+00	2.50E-02	7.00E+03	2.50E-02	0.00E+00
9	MXEG	6	7	0.00E+00	0.00E+00	5.00E-01	7.00E+03	2.94E-01	2.11E-01
10	MXEG	8	9	0.00E+00	0.00E+00	5.00E-01	7.00E+03	4.00E-01	4.95E-02
11	MXEG	10	11	0.00E+00	0.00E+00	5.00E-01	7.00E+03	6.00E-03	1.21E+00
12	DMFS	0	0	0.00E+00	0.00E+00	0.00E+00	0.00E+00	0.00E+00	0.00E+00
13	BLNK	0	0	0.00E+00	0.00E+00	0.00E+00	0.00E+00	0.00E+00	0.00E+00
14	CONF	1	0	0.00E+00	0.00E+00	0.00E+00	0.00E+00	0.00E+00	0.00E+00
15	BLNK	0	0	0.00E+00	0.00E+00	0.00E+00	0.00E+00	0.00E+00	0.00E+00
16	MXEG	6	7	0.00E+00	0.00E+00	5.00E-01	7.00E+03	2.94E-01	2.11E-01
17	MXEG	8	9	0.00E+00	0.00E+00	5.00E-01	7.00E+03	4.00E-01	4.95E-02
18	BLNK	0	0	0.00E+00	0.00E+00	0.00E+00	0.00E+00	0.00E+00	0.00E+00
19	BLNK	0	0	0.00E+00	0.00E+00	0.00E+00	0.00E+00	0.00E+00	0.00E+00
20	OPDX	0	1	1.68E-01	2.91E-01	0.00E+00	4.85E-02	-8.18E-02	2.29E-07
21	OPDX	0	1	3.54E-01	6.12E-01	0.00E+00	7.76E-02	-1.87E-01	1.92E-06
22	OPDX	0	1	4.71E-01	8.16E-01	0.00E+00	4.85E-02	3.81E-01	4.98E-06
23	OPDX	0	1	3.36E-01	0.00E+00	0.00E+00	4.85E-02	-8.18E-02	2.29E-07
24	OPDX	0	1	7.07E-01	0.00E+00	0.00E+00	7.76E-02	-1.87E-01	1.92E-06
25	OPDX	0	1	9.42E-01	0.00E+00	0.00E+00	4.85E-02	3.81E-01	4.98E-06
26	OPDX	0	1	1.68E-01	-2.91E-01	0.00E+00	4.85E-02	-8.18E-02	2.29E-07
27	OPDX	0	1	3.54E-01	-6.12E-01	0.00E+00	7.76E-02	-1.87E-01	1.92E-06
28	OPDX	0	1	4.71E-01	-8.16E-01	0.00E+00	4.85E-02	3.81E-01	4.98E-06
29	OPDX	0	1	-1.68E-01	-2.91E-01	0.00E+00	4.85E-02	-8.18E-02	2.29E-07
30	OPDX	0	1	-3.54E-01	-6.12E-01	0.00E+00	7.76E-02	-1.87E-01	1.92E-06
31	OPDX	0	1	-4.71E-01	-8.16E-01	0.00E+00	4.85E-02	3.81E-01	4.98E-06
32	OPDX	0	1	-3.36E-01	2.57E-16	0.00E+00	4.85E-02	-8.18E-02	2.29E-07
33	OPDX	0	1	-7.07E-01	5.41E-16	0.00E+00	7.76E-02	-1.87E-01	1.92E-06
34	OPDX	0	1	-9.42E-01	7.21E-16	0.00E+00	4.85E-02	3.81E-01	4.98E-06
35	OPDX	0	1	-1.68E-01	2.91E-01	0.00E+00	4.85E-02	-8.18E-02	2.29E-07
36	OPDX	0	1	-3.54E-01	6.12E-01	0.00E+00	7.76E-02	-1.87E-01	1.92E-06
37	OPDX	0	1	-4.71E-01	8.16E-01	0.00E+00	4.85E-02	3.81E-01	4.98E-06
38	OPDX	0	1	1.68E-01	2.91E-01	0.00E+00	4.85E-02	-8.18E-02	2.29E-07
39	OPDX	0	1	3.54E-01	6.12E-01	0.00E+00	7.76E-02	-1.87E-01	1.92E-06
40	OPDX	0	1	4.71E-01	8.16E-01	0.00E+00	4.85E-02	3.81E-01	4.98E-06
41	OPDX	0	1	3.36E-01	0.00E+00	0.00E+00	4.85E-02	-8.18E-02	2.29E-07
42	OPDX	0	1	7.07E-01	0.00E+00	0.00E+00	7.76E-02	-1.87E-01	1.92E-06
43	OPDX	0	1	9.42E-01	0.00E+00	0.00E+00	4.85E-02	3.81E-01	4.98E-06
44	OPDX	0	1	1.68E-01	-2.91E-01	0.00E+00	4.85E-02	-8.18E-02	2.29E-07

45	OPDX	0	1	3.54E-01	-6.12E-01	0.00E+00	7.76E-02	-1.87E-01	1.92E-06
46	OPDX	0	1	4.71E-01	-8.16E-01	0.00E+00	4.85E-02	3.81E-01	4.98E-06
47	OPDX	0	1	-1.68E-01	-2.91E-01	0.00E+00	4.85E-02	-8.18E-02	2.29E-07
48	OPDX	0	1	-3.54E-01	-6.12E-01	0.00E+00	7.76E-02	-1.87E-01	1.92E-06
49	OPDX	0	1	-4.71E-01	-8.16E-01	0.00E+00	4.85E-02	3.81E-01	4.98E-06
50	OPDX	0	1	-3.36E-01	2.57E-16	0.00E+00	4.85E-02	-8.18E-02	2.29E-07
51	OPDX	0	1	-7.07E-01	5.41E-16	0.00E+00	7.76E-02	-1.87E-01	1.92E-06
52	OPDX	0	1	-9.42E-01	7.21E-16	0.00E+00	4.85E-02	3.81E-01	4.98E-06
53	OPDX	0	1	-1.68E-01	2.91E-01	0.00E+00	4.85E-02	-8.18E-02	2.29E-07
54	OPDX	0	1	-3.54E-01	6.12E-01	0.00E+00	7.76E-02	-1.87E-01	1.92E-06
55	OPDX	0	1	-4.71E-01	8.16E-01	0.00E+00	4.85E-02	3.81E-01	4.98E-06
56	OPDX	0	1	1.68E-01	2.91E-01	0.00E+00	4.85E-02	-8.18E-02	2.29E-07
57	OPDX	0	1	3.54E-01	6.12E-01	0.00E+00	7.76E-02	-1.87E-01	1.92E-06
58	OPDX	0	1	4.71E-01	8.16E-01	0.00E+00	4.85E-02	3.81E-01	4.98E-06
59	OPDX	0	1	3.36E-01	0.00E+00	0.00E+00	4.85E-02	-8.18E-02	2.29E-07
60	OPDX	0	1	7.07E-01	0.00E+00	0.00E+00	7.76E-02	-1.87E-01	1.92E-06
61	OPDX	0	1	9.42E-01	0.00E+00	0.00E+00	4.85E-02	3.81E-01	4.98E-06
62	OPDX	0	1	1.68E-01	-2.91E-01	0.00E+00	4.85E-02	-8.18E-02	2.29E-07
63	OPDX	0	1	3.54E-01	-6.12E-01	0.00E+00	7.76E-02	-1.87E-01	1.92E-06
64	OPDX	0	1	4.71E-01	-8.16E-01	0.00E+00	4.85E-02	3.81E-01	4.98E-06
65	OPDX	0	1	-1.68E-01	-2.91E-01	0.00E+00	4.85E-02	-8.18E-02	2.29E-07
66	OPDX	0	1	-3.54E-01	-6.12E-01	0.00E+00	7.76E-02	-1.87E-01	1.92E-06
67	OPDX	0	1	-4.71E-01	-8.16E-01	0.00E+00	4.85E-02	3.81E-01	4.98E-06
68	OPDX	0	1	-3.36E-01	2.57E-16	0.00E+00	4.85E-02	-8.18E-02	2.29E-07
69	OPDX	0	1	-7.07E-01	5.41E-16	0.00E+00	7.76E-02	-1.87E-01	1.92E-06
70	OPDX	0	1	-9.42E-01	7.21E-16	0.00E+00	4.85E-02	3.81E-01	4.98E-06
71	OPDX	0	1	-1.68E-01	2.91E-01	0.00E+00	4.85E-02	-8.18E-02	2.29E-07
72	OPDX	0	1	-3.54E-01	6.12E-01	0.00E+00	7.76E-02	-1.87E-01	1.92E-06
73	OPDX	0	1	-4.71E-01	8.16E-01	0.00E+00	4.85E-02	3.81E-01	4.98E-06
74	OPDX	0	2	1.68E-01	2.91E-01	0.00E+00	4.85E-02	-2.22E-01	1.69E-06
75	OPDX	0	2	3.54E-01	6.12E-01	0.00E+00	7.76E-02	-1.83E-01	1.83E-06
76	OPDX	0	2	4.71E-01	8.16E-01	0.00E+00	4.85E-02	5.14E-01	9.07E-06
77	OPDX	0	2	3.36E-01	0.00E+00	0.00E+00	4.85E-02	-2.22E-01	1.69E-06
78	OPDX	0	2	7.07E-01	0.00E+00	0.00E+00	7.76E-02	-1.83E-01	1.83E-06
79	OPDX	0	2	9.42E-01	0.00E+00	0.00E+00	4.85E-02	5.14E-01	9.07E-06
80	OPDX	0	2	1.68E-01	-2.91E-01	0.00E+00	4.85E-02	-2.22E-01	1.69E-06
81	OPDX	0	2	3.54E-01	-6.12E-01	0.00E+00	7.76E-02	-1.83E-01	1.83E-06
82	OPDX	0	2	4.71E-01	-8.16E-01	0.00E+00	4.85E-02	5.14E-01	9.07E-06
83	OPDX	0	2	-1.68E-01	-2.91E-01	0.00E+00	4.85E-02	-2.22E-01	1.69E-06
84	OPDX	0	2	-3.54E-01	-6.12E-01	0.00E+00	7.76E-02	-1.83E-01	1.83E-06
85	OPDX	0	2	-4.71E-01	-8.16E-01	0.00E+00	4.85E-02	5.14E-01	9.07E-06
86	OPDX	0	2	-3.36E-01	2.57E-16	0.00E+00	4.85E-02	-2.22E-01	1.69E-06
87	OPDX	0	2	-7.07E-01	5.41E-16	0.00E+00	7.76E-02	-1.83E-01	1.83E-06
88	OPDX	0	2	-9.42E-01	7.21E-16	0.00E+00	4.85E-02	5.14E-01	9.07E-06
89	OPDX	0	2	-1.68E-01	2.91E-01	0.00E+00	4.85E-02	-2.22E-01	1.69E-06
90	OPDX	0	2	-3.54E-01	6.12E-01	0.00E+00	7.76E-02	-1.83E-01	1.83E-06
91	OPDX	0	2	-4.71E-01	8.16E-01	0.00E+00	4.85E-02	5.14E-01	9.07E-06

92	OPDX	0	2	1.68E-01	2.91E-01	0.00E+00	4.85E-02	-2.22E-01	1.69E-06
93	OPDX	0	2	3.54E-01	6.12E-01	0.00E+00	7.76E-02	-1.83E-01	1.83E-06
94	OPDX	0	2	4.71E-01	8.16E-01	0.00E+00	4.85E-02	5.14E-01	9.07E-06
95	OPDX	0	2	3.36E-01	0.00E+00	0.00E+00	4.85E-02	-2.22E-01	1.69E-06
96	OPDX	0	2	7.07E-01	0.00E+00	0.00E+00	7.76E-02	-1.83E-01	1.83E-06
97	OPDX	0	2	9.42E-01	0.00E+00	0.00E+00	4.85E-02	5.14E-01	9.07E-06
98	OPDX	0	2	1.68E-01	-2.91E-01	0.00E+00	4.85E-02	-2.22E-01	1.69E-06
99	OPDX	0	2	3.54E-01	-6.12E-01	0.00E+00	7.76E-02	-1.83E-01	1.83E-06
100	OPDX	0	2	4.71E-01	-8.16E-01	0.00E+00	4.85E-02	5.14E-01	9.07E-06
101	OPDX	0	2	-1.68E-01	-2.91E-01	0.00E+00	4.85E-02	-2.22E-01	1.69E-06
102	OPDX	0	2	-3.54E-01	-6.12E-01	0.00E+00	7.76E-02	-1.83E-01	1.83E-06
103	OPDX	0	2	-4.71E-01	-8.16E-01	0.00E+00	4.85E-02	5.14E-01	9.07E-06
104	OPDX	0	2	-3.36E-01	2.57E-16	0.00E+00	4.85E-02	-2.22E-01	1.69E-06
105	OPDX	0	2	-7.07E-01	5.41E-16	0.00E+00	7.76E-02	-1.83E-01	1.83E-06
106	OPDX	0	2	-9.42E-01	7.21E-16	0.00E+00	4.85E-02	5.14E-01	9.07E-06
107	OPDX	0	2	-1.68E-01	2.91E-01	0.00E+00	4.85E-02	-2.22E-01	1.69E-06
108	OPDX	0	2	-3.54E-01	6.12E-01	0.00E+00	7.76E-02	-1.83E-01	1.83E-06
109	OPDX	0	2	-4.71E-01	8.16E-01	0.00E+00	4.85E-02	5.14E-01	9.07E-06
110	OPDX	0	2	1.68E-01	2.91E-01	0.00E+00	4.85E-02	-2.22E-01	1.69E-06
111	OPDX	0	2	3.54E-01	6.12E-01	0.00E+00	7.76E-02	-1.83E-01	1.83E-06
112	OPDX	0	2	4.71E-01	8.16E-01	0.00E+00	4.85E-02	5.14E-01	9.07E-06
113	OPDX	0	2	3.36E-01	0.00E+00	0.00E+00	4.85E-02	-2.22E-01	1.69E-06
114	OPDX	0	2	7.07E-01	0.00E+00	0.00E+00	7.76E-02	-1.83E-01	1.83E-06
115	OPDX	0	2	9.42E-01	0.00E+00	0.00E+00	4.85E-02	5.14E-01	9.07E-06
116	OPDX	0	2	1.68E-01	-2.91E-01	0.00E+00	4.85E-02	-2.22E-01	1.69E-06
117	OPDX	0	2	3.54E-01	-6.12E-01	0.00E+00	7.76E-02	-1.83E-01	1.83E-06
118	OPDX	0	2	4.71E-01	-8.16E-01	0.00E+00	4.85E-02	5.14E-01	9.07E-06
119	OPDX	0	2	-1.68E-01	-2.91E-01	0.00E+00	4.85E-02	-2.22E-01	1.69E-06
120	OPDX	0	2	-3.54E-01	-6.12E-01	0.00E+00	7.76E-02	-1.83E-01	1.83E-06
121	OPDX	0	2	-4.71E-01	-8.16E-01	0.00E+00	4.85E-02	5.14E-01	9.07E-06
122	OPDX	0	2	-3.36E-01	2.57E-16	0.00E+00	4.85E-02	-2.22E-01	1.69E-06
123	OPDX	0	2	-7.07E-01	5.41E-16	0.00E+00	7.76E-02	-1.83E-01	1.83E-06
124	OPDX	0	2	-9.42E-01	7.21E-16	0.00E+00	4.85E-02	5.14E-01	9.07E-06
125	OPDX	0	2	-1.68E-01	2.91E-01	0.00E+00	4.85E-02	-2.22E-01	1.69E-06
126	OPDX	0	2	-3.54E-01	6.12E-01	0.00E+00	7.76E-02	-1.83E-01	1.83E-06
127	OPDX	0	2	-4.71E-01	8.16E-01	0.00E+00	4.85E-02	5.14E-01	9.07E-06
128	CONF	2	0	0.00E+00	0.00E+00	0.00E+00	0.00E+00	0.00E+00	0.00E+00
129	LACL	0	0	0.00E+00	0.00E+00	0.00E+00	5.00E+05	0.00E+00	0.00E+00
130	EFFL	0	1	0.00E+00	0.00E+00	1.00E+00	5.00E+05	1.21E+00	1.56E+01
131	SPHA	1	1	0.00E+00	0.00E+00	0.00E+00	5.00E+05	0.00E+00	7.77E-02
132	SPHA	1	2	0.00E+00	0.00E+00	0.00E+00	5.00E+05	0.00E+00	7.70E-02
133	EFFL	0	2	0.00E+00	0.00E+00	1.00E+00	5.00E+05	1.21E+00	1.50E+01
134	AXCL	0	0	0.00E+00	0.00E+00	0.00E+00	5.00E+07	-1.66E-03	9.76E-02
135	MCOL	2	2	0.00E+00	0.00E+00	2.50E-02	7.00E+03	2.50E-02	0.00E+00
136	MXEG	6	7	0.00E+00	0.00E+00	5.00E-01	7.00E+03	2.94E-01	2.11E-01
137	MXEG	8	9	0.00E+00	0.00E+00	5.00E-01	7.00E+03	4.00E-01	4.95E-02
138	MXEG	10	11	0.00E+00	0.00E+00	5.00E-01	7.00E+03	0.00E+00	1.24E+00

139	BLNK	0	0	0.00E+00	0.00E+00	0.00E+00	0.00E+00	0.00E+00	0.00E+00
140	CONF	2	0	0.00E+00	0.00E+00	0.00E+00	0.00E+00	0.00E+00	0.00E+00
141	EFFL	0	1	0.00E+00	0.00E+00	1.00E+00	5.00E+05	1.21E+00	1.56E+01
142	EFFL	0	2	0.00E+00	0.00E+00	1.00E+00	5.00E+05	1.21E+00	1.50E+01
143	BLNK	0	0	0.00E+00	0.00E+00	0.00E+00	0.00E+00	0.00E+00	0.00E+00
144	MXEG	6	7	0.00E+00	0.00E+00	5.00E-01	7.00E+03	2.94E-01	2.11E-01
145	MXEG	8	9	0.00E+00	0.00E+00	5.00E-01	7.00E+03	4.00E-01	4.95E-02
146	BLNK	0	0	0.00E+00	0.00E+00	0.00E+00	0.00E+00	0.00E+00	0.00E+00
147	BLNK	0	0	0.00E+00	0.00E+00	0.00E+00	0.00E+00	0.00E+00	0.00E+00
148	OPDX	0	1	1.68E-01	2.91E-01	0.00E+00	4.85E-02	1.69E-01	9.84E-07
149	OPDX	0	1	3.54E-01	6.12E-01	0.00E+00	7.76E-02	1.45E-01	1.15E-06
150	OPDX	0	1	4.71E-01	8.16E-01	0.00E+00	1.00E+00	2.24E-01	3.55E-05
151	OPDX	0	1	3.36E-01	0.00E+00	0.00E+00	4.85E-02	-3.66E-01	4.59E-06
152	OPDX	0	1	7.07E-01	0.00E+00	0.00E+00	7.76E-02	-6.25E-01	2.14E-05
153	OPDX	0	1	9.42E-01	0.00E+00	0.00E+00	4.85E-02	-1.96E-01	1.32E-06
154	OPDX	0	1	1.68E-01	-2.91E-01	0.00E+00	4.85E-02	-7.70E-01	2.03E-05
155	OPDX	0	1	3.54E-01	-6.12E-01	0.00E+00	7.76E-02	-7.37E-01	2.98E-05
156	OPDX	0	1	4.71E-01	-8.16E-01	0.00E+00	1.00E+00	7.44E-01	3.91E-04
157	OPDX	0	1	-1.68E-01	-2.91E-01	0.00E+00	4.85E-02	-7.36E-01	1.86E-05
158	OPDX	0	1	-3.54E-01	-6.12E-01	0.00E+00	7.76E-02	-6.68E-01	2.44E-05
159	OPDX	0	1	-4.71E-01	-8.16E-01	0.00E+00	1.00E+00	8.35E-01	4.94E-04
160	OPDX	0	1	-3.36E-01	2.57E-16	0.00E+00	4.85E-02	-2.98E-01	3.05E-06
161	OPDX	0	1	-7.07E-01	5.41E-16	0.00E+00	7.76E-02	-4.84E-01	1.29E-05
162	OPDX	0	1	-9.42E-01	7.21E-16	0.00E+00	4.85E-02	-1.16E-02	4.64E-09
163	OPDX	0	1	-1.68E-01	2.91E-01	0.00E+00	4.85E-02	2.03E-01	1.42E-06
164	OPDX	0	1	-3.54E-01	6.12E-01	0.00E+00	7.76E-02	2.15E-01	2.54E-06
165	OPDX	0	1	-4.71E-01	8.16E-01	0.00E+00	1.00E+00	3.17E-01	7.09E-05
166	OPDX	0	1	1.68E-01	2.91E-01	0.00E+00	4.85E-02	1.69E-01	9.84E-07
167	OPDX	0	1	3.54E-01	6.12E-01	0.00E+00	7.76E-02	1.45E-01	1.15E-06
168	OPDX	0	1	4.71E-01	8.16E-01	0.00E+00	1.00E+00	2.24E-01	3.55E-05
169	OPDX	0	1	3.36E-01	0.00E+00	0.00E+00	4.85E-02	-3.66E-01	4.59E-06
170	OPDX	0	1	7.07E-01	0.00E+00	0.00E+00	7.76E-02	-6.25E-01	2.14E-05
171	OPDX	0	1	9.42E-01	0.00E+00	0.00E+00	4.85E-02	-1.96E-01	1.32E-06
172	OPDX	0	1	1.68E-01	-2.91E-01	0.00E+00	4.85E-02	-7.70E-01	2.03E-05
173	OPDX	0	1	3.54E-01	-6.12E-01	0.00E+00	7.76E-02	-7.37E-01	2.98E-05
174	OPDX	0	1	4.71E-01	-8.16E-01	0.00E+00	1.00E+00	7.44E-01	3.91E-04
175	OPDX	0	1	-1.68E-01	-2.91E-01	0.00E+00	4.85E-02	-7.36E-01	1.86E-05
176	OPDX	0	1	-3.54E-01	-6.12E-01	0.00E+00	7.76E-02	-6.68E-01	2.44E-05
177	OPDX	0	1	-4.71E-01	-8.16E-01	0.00E+00	4.85E-02	8.35E-01	2.39E-05
178	OPDX	0	1	-3.36E-01	2.57E-16	0.00E+00	4.85E-02	-2.98E-01	3.05E-06
179	OPDX	0	1	-7.07E-01	5.41E-16	0.00E+00	7.76E-02	-4.84E-01	1.29E-05
180	OPDX	0	1	-9.42E-01	7.21E-16	0.00E+00	4.85E-02	-1.16E-02	4.64E-09
181	OPDX	0	1	-1.68E-01	2.91E-01	0.00E+00	4.85E-02	2.03E-01	1.42E-06
182	OPDX	0	1	-3.54E-01	6.12E-01	0.00E+00	7.76E-02	2.15E-01	2.54E-06
183	OPDX	0	1	-4.71E-01	8.16E-01	0.00E+00	1.00E+00	3.17E-01	7.09E-05
184	OPDX	0	1	1.68E-01	2.91E-01	0.00E+00	4.85E-02	1.69E-01	9.84E-07
185	OPDX	0	1	3.54E-01	6.12E-01	0.00E+00	7.76E-02	1.45E-01	1.15E-06

186	OPDX	0	1	4.71E-01	8.16E-01	0.00E+00	1.00E+00	2.24E-01	3.55E-05
187	OPDX	0	1	3.36E-01	0.00E+00	0.00E+00	4.85E-02	-3.66E-01	4.59E-06
188	OPDX	0	1	7.07E-01	0.00E+00	0.00E+00	7.76E-02	-6.25E-01	2.14E-05
189	OPDX	0	1	9.42E-01	0.00E+00	0.00E+00	4.85E-02	-1.96E-01	1.32E-06
190	OPDX	0	1	1.68E-01	-2.91E-01	0.00E+00	4.85E-02	-7.70E-01	2.03E-05
191	OPDX	0	1	3.54E-01	-6.12E-01	0.00E+00	7.76E-02	-7.37E-01	2.98E-05
192	OPDX	0	1	4.71E-01	-8.16E-01	0.00E+00	1.00E+00	7.44E-01	3.91E-04
193	OPDX	0	1	-1.68E-01	-2.91E-01	0.00E+00	4.85E-02	-7.36E-01	1.86E-05
194	OPDX	0	1	-3.54E-01	-6.12E-01	0.00E+00	7.76E-02	-6.68E-01	2.44E-05
195	OPDX	0	1	-4.71E-01	-8.16E-01	0.00E+00	1.00E+00	8.35E-01	4.94E-04
196	OPDX	0	1	-3.36E-01	2.57E-16	0.00E+00	4.85E-02	-2.98E-01	3.05E-06
197	OPDX	0	1	-7.07E-01	5.41E-16	0.00E+00	7.76E-02	-4.84E-01	1.29E-05
198	OPDX	0	1	-9.42E-01	7.21E-16	0.00E+00	4.85E-02	-1.16E-02	4.64E-09
199	OPDX	0	1	-1.68E-01	2.91E-01	0.00E+00	4.85E-02	2.03E-01	1.42E-06
200	OPDX	0	1	-3.54E-01	6.12E-01	0.00E+00	7.76E-02	2.15E-01	2.54E-06
201	OPDX	0	1	-4.71E-01	8.16E-01	0.00E+00	1.00E+00	3.17E-01	7.09E-05
202	OPDX	0	2	1.68E-01	2.91E-01	0.00E+00	4.85E-02	-8.16E-01	2.28E-05
203	OPDX	0	2	3.54E-01	6.12E-01	0.00E+00	7.76E-02	-6.04E-01	2.00E-05
204	OPDX	0	2	4.71E-01	8.16E-01	0.00E+00	4.85E-02	-3.19E-01	3.48E-06
205	OPDX	0	2	3.36E-01	0.00E+00	0.00E+00	4.85E-02	########	6.95E-05
206	OPDX	0	2	7.07E-01	0.00E+00	0.00E+00	7.76E-02	########	1.29E-04
207	OPDX	0	2	9.42E-01	0.00E+00	0.00E+00	4.85E-02	-9.77E-01	3.27E-05
208	OPDX	0	2	1.68E-01	-2.91E-01	0.00E+00	4.85E-02	########	1.24E-04
209	OPDX	0	2	3.54E-01	-6.12E-01	0.00E+00	7.76E-02	########	1.86E-04
210	OPDX	0	2	4.71E-01	-8.16E-01	0.00E+00	1.00E+00	-3.44E-01	8.35E-05
211	OPDX	0	2	-1.68E-01	-2.91E-01	0.00E+00	4.85E-02	########	1.20E-04
212	OPDX	0	2	-3.54E-01	-6.12E-01	0.00E+00	7.76E-02	########	1.72E-04
213	OPDX	0	2	-4.71E-01	-8.16E-01	0.00E+00	1.00E+00	-2.52E-01	4.50E-05
214	OPDX	0	2	-3.36E-01	2.57E-16	0.00E+00	4.85E-02	########	6.31E-05
215	OPDX	0	2	-7.07E-01	5.41E-16	0.00E+00	7.76E-02	########	1.07E-04
216	OPDX	0	2	-9.42E-01	7.21E-16	0.00E+00	4.85E-02	-7.94E-01	2.16E-05
217	OPDX	0	2	-1.68E-01	2.91E-01	0.00E+00	4.85E-02	-7.82E-01	2.10E-05
218	OPDX	0	2	-3.54E-01	6.12E-01	0.00E+00	7.76E-02	-5.34E-01	1.57E-05
219	OPDX	0	2	-4.71E-01	8.16E-01	0.00E+00	4.85E-02	-2.27E-01	1.76E-06
220	OPDX	0	2	1.68E-01	2.91E-01	0.00E+00	4.85E-02	-8.16E-01	2.28E-05
221	OPDX	0	2	3.54E-01	6.12E-01	0.00E+00	7.76E-02	-6.04E-01	2.00E-05
222	OPDX	0	2	4.71E-01	8.16E-01	0.00E+00	4.85E-02	-3.19E-01	3.48E-06
223	OPDX	0	2	3.36E-01	0.00E+00	0.00E+00	4.85E-02	########	6.95E-05
224	OPDX	0	2	7.07E-01	0.00E+00	0.00E+00	7.76E-02	########	1.29E-04
225	OPDX	0	2	9.42E-01	0.00E+00	0.00E+00	4.85E-02	-9.77E-01	3.27E-05
226	OPDX	0	2	1.68E-01	-2.91E-01	0.00E+00	4.85E-02	########	1.24E-04
227	OPDX	0	2	3.54E-01	-6.12E-01	0.00E+00	7.76E-02	########	1.86E-04
228	OPDX	0	2	4.71E-01	-8.16E-01	0.00E+00	1.00E+00	-3.44E-01	8.35E-05
229	OPDX	0	2	-1.68E-01	-2.91E-01	0.00E+00	4.85E-02	########	1.20E-04
230	OPDX	0	2	-3.54E-01	-6.12E-01	0.00E+00	7.76E-02	########	1.72E-04
231	OPDX	0	2	-4.71E-01	-8.16E-01	0.00E+00	1.00E+00	-2.52E-01	4.50E-05
232	OPDX	0	2	-3.36E-01	2.57E-16	0.00E+00	4.85E-02	########	6.31E-05

233	OPDX	0	2	-7.07E-01	5.41E-16	0.00E+00	7.76E-02	########	1.07E-04
234	OPDX	0	2	-9.42E-01	7.21E-16	0.00E+00	4.85E-02	-7.94E-01	2.16E-05
235	OPDX	0	2	-1.68E-01	2.91E-01	0.00E+00	4.85E-02	-7.82E-01	2.10E-05
236	OPDX	0	2	-3.54E-01	6.12E-01	0.00E+00	7.76E-02	-5.34E-01	1.57E-05
237	OPDX	0	2	-4.71E-01	8.16E-01	0.00E+00	4.85E-02	-2.27E-01	1.76E-06
238	OPDX	0	2	1.68E-01	2.91E-01	0.00E+00	4.85E-02	-8.16E-01	2.28E-05
239	OPDX	0	2	3.54E-01	6.12E-01	0.00E+00	7.76E-02	-6.04E-01	2.00E-05
240	OPDX	0	2	4.71E-01	8.16E-01	0.00E+00	4.85E-02	-3.19E-01	3.48E-06
241	OPDX	0	2	3.36E-01	0.00E+00	0.00E+00	4.85E-02	########	6.95E-05
242	OPDX	0	2	7.07E-01	0.00E+00	0.00E+00	7.76E-02	########	1.29E-04
243	OPDX	0	2	9.42E-01	0.00E+00	0.00E+00	4.85E-02	-9.77E-01	3.27E-05
244	OPDX	0	2	1.68E-01	-2.91E-01	0.00E+00	4.85E-02	########	1.24E-04
245	OPDX	0	2	3.54E-01	-6.12E-01	0.00E+00	7.76E-02	########	1.86E-04
246	OPDX	0	2	4.71E-01	-8.16E-01	0.00E+00	4.85E-02	-3.44E-01	4.05E-06
247	OPDX	0	2	-1.68E-01	-2.91E-01	0.00E+00	4.85E-02	########	1.20E-04
248	OPDX	0	2	-3.54E-01	-6.12E-01	0.00E+00	7.76E-02	########	1.72E-04
249	OPDX	0	2	-4.71E-01	-8.16E-01	0.00E+00	1.00E+00	-2.52E-01	4.50E-05
250	OPDX	0	2	-3.36E-01	2.57E-16	0.00E+00	4.85E-02	########	6.31E-05
251	OPDX	0	2	-7.07E-01	5.41E-16	0.00E+00	7.76E-02	########	1.07E-04
252	OPDX	0	2	-9.42E-01	7.21E-16	0.00E+00	4.85E-02	-7.94E-01	2.16E-05
253	OPDX	0	2	-1.68E-01	2.91E-01	0.00E+00	4.85E-02	-7.82E-01	2.10E-05
254	OPDX	0	2	-3.54E-01	6.12E-01	0.00E+00	7.76E-02	-5.34E-01	1.57E-05
255	OPDX	0	2	-4.71E-01	8.16E-01	0.00E+00	4.85E-02	-2.27E-01	1.76E-06
256	CONF	3	0	0.00E+00	0.00E+00	0.00E+00	0.00E+00	0.00E+00	0.00E+00
257	LACL	0	0	0.00E+00	0.00E+00	0.00E+00	5.00E+05	0.00E+00	0.00E+00
258	SPHA	1	1	0.00E+00	0.00E+00	0.00E+00	5.00E+05	6.22E-04	28.3E+00
259	SPHA	1	2	0.00E+00	0.00E+00	0.00E+00	5.00E+05	6.18E-04	25.6E+00
260	EFFL	0	1	0.00E+00	0.00E+00	1.00E+00	5.00E+05	9.72E-01	2.84E-01
261	EFFL	0	2	0.00E+00	0.00E+00	1.00E+00	5.00E+05	9.70E-01	3.26E-01
262	AXCL	0	0	0.00E+00	0.00E+00	0.00E+00	5.00E+07	-8.86E-04	2.78E-02
263	MCOV	1	3	0.00E+00	0.00E+00	8.00E-02	7.00E+03	7.60E-02	7.92E-05
264	MXEG	6	7	0.00E+00	0.00E+00	5.00E-01	7.00E+03	2.94E-01	2.11E-01
265	MXEG	8	9	0.00E+00	0.00E+00	5.00E-01	7.00E+03	4.00E-01	4.95E-02
266	MXEG	10	11	0.00E+00	0.00E+00	5.00E-01	7.00E+03	7.60E-02	8.90E-01
267	BLNK	0	0	0.00E+00	0.00E+00	0.00E+00	0.00E+00	0.00E+00	0.00E+00
268	CONF	3	0	0.00E+00	0.00E+00	0.00E+00	0.00E+00	0.00E+00	0.00E+00
269	EFFL	0	1	0.00E+00	0.00E+00	1.00E+00	5.00E+05	9.72E-01	2.84E-01
270	EFFL	0	2	0.00E+00	0.00E+00	1.00E+00	5.00E+05	9.70E-01	3.26E-01
271	BLNK	0	0	0.00E+00	0.00E+00	0.00E+00	0.00E+00	0.00E+00	0.00E+00
272	MXEG	6	7	0.00E+00	0.00E+00	5.00E-01	7.00E+03	2.94E-01	2.11E-01
273	MXEG	8	9	0.00E+00	0.00E+00	5.00E-01	7.00E+03	4.00E-01	4.95E-02
274	BLNK	0	0	0.00E+00	0.00E+00	0.00E+00	0.00E+00	0.00E+00	0.00E+00
275	BLNK	0	0	0.00E+00	0.00E+00	0.00E+00	0.00E+00	0.00E+00	0.00E+00
276	OPDX	0	1	1.68E-01	2.91E-01	0.00E+00	4.85E-02	-5.60E-01	1.07E-05
277	OPDX	0	1	3.54E-01	6.12E-01	0.00E+00	7.76E-02	-3.93E-01	8.47E-06
278	OPDX	0	1	4.71E-01	8.16E-01	0.00E+00	4.85E-02	1.19E+00	4.84E-05
279	OPDX	0	1	3.36E-01	0.00E+00	0.00E+00	4.85E-02	-5.60E-01	1.07E-05

280	OPDX	0	1	7.07E-01	0.00E+00	0.00E+00	7.76E-02	-3.93E-01	8.47E-06
281	OPDX	0	1	9.42E-01	0.00E+00	0.00E+00	4.85E-02	1.19E+00	4.84E-05
282	OPDX	0	1	1.68E-01	-2.91E-01	0.00E+00	4.85E-02	-5.60E-01	1.07E-05
283	OPDX	0	1	3.54E-01	-6.12E-01	0.00E+00	7.76E-02	-3.93E-01	8.47E-06
284	OPDX	0	1	4.71E-01	-8.16E-01	0.00E+00	4.85E-02	1.19E+00	4.84E-05
285	OPDX	0	1	-1.68E-01	-2.91E-01	0.00E+00	4.85E-02	-5.60E-01	1.07E-05
286	OPDX	0	1	-3.54E-01	-6.12E-01	0.00E+00	7.76E-02	-3.93E-01	8.47E-06
287	OPDX	0	1	-4.71E-01	-8.16E-01	0.00E+00	4.85E-02	1.19E+00	4.84E-05
288	OPDX	0	1	-3.36E-01	2.57E-16	0.00E+00	4.85E-02	-5.60E-01	1.07E-05
289	OPDX	0	1	-7.07E-01	5.41E-16	0.00E+00	7.76E-02	-3.93E-01	8.47E-06
290	OPDX	0	1	-9.42E-01	7.21E-16	0.00E+00	4.85E-02	1.19E+00	4.84E-05
291	OPDX	0	1	-1.68E-01	2.91E-01	0.00E+00	4.85E-02	-5.60E-01	1.07E-05
292	OPDX	0	1	-3.54E-01	6.12E-01	0.00E+00	7.76E-02	-3.93E-01	8.47E-06
293	OPDX	0	1	-4.71E-01	8.16E-01	0.00E+00	4.85E-02	1.19E+00	4.84E-05
294	OPDX	0	1	1.68E-01	2.91E-01	0.00E+00	4.85E-02	-5.60E-01	1.07E-05
295	OPDX	0	1	3.54E-01	6.12E-01	0.00E+00	7.76E-02	-3.93E-01	8.47E-06
296	OPDX	0	1	4.71E-01	8.16E-01	0.00E+00	4.85E-02	1.19E+00	4.84E-05
297	OPDX	0	1	3.36E-01	0.00E+00	0.00E+00	4.85E-02	-5.60E-01	1.07E-05
298	OPDX	0	1	7.07E-01	0.00E+00	0.00E+00	7.76E-02	-3.93E-01	8.47E-06
299	OPDX	0	1	9.42E-01	0.00E+00	0.00E+00	4.85E-02	1.19E+00	4.84E-05
300	OPDX	0	1	1.68E-01	-2.91E-01	0.00E+00	4.85E-02	-5.60E-01	1.07E-05
301	OPDX	0	1	3.54E-01	-6.12E-01	0.00E+00	7.76E-02	-3.93E-01	8.47E-06
302	OPDX	0	1	4.71E-01	-8.16E-01	0.00E+00	4.85E-02	1.19E+00	4.84E-05
303	OPDX	0	1	-1.68E-01	-2.91E-01	0.00E+00	4.85E-02	-5.60E-01	1.07E-05
304	OPDX	0	1	-3.54E-01	-6.12E-01	0.00E+00	7.76E-02	-3.93E-01	8.47E-06
305	OPDX	0	1	-4.71E-01	-8.16E-01	0.00E+00	4.85E-02	1.19E+00	4.84E-05
306	OPDX	0	1	-3.36E-01	2.57E-16	0.00E+00	4.85E-02	-5.60E-01	1.07E-05
307	OPDX	0	1	-7.07E-01	5.41E-16	0.00E+00	7.76E-02	-3.93E-01	8.47E-06
308	OPDX	0	1	-9.42E-01	7.21E-16	0.00E+00	4.85E-02	1.19E+00	4.84E-05
309	OPDX	0	1	-1.68E-01	2.91E-01	0.00E+00	4.85E-02	-5.60E-01	1.07E-05
310	OPDX	0	1	-3.54E-01	6.12E-01	0.00E+00	7.76E-02	-3.93E-01	8.47E-06
311	OPDX	0	1	-4.71E-01	8.16E-01	0.00E+00	4.85E-02	1.19E+00	4.84E-05
312	OPDX	0	1	1.68E-01	2.91E-01	0.00E+00	4.85E-02	-5.60E-01	1.07E-05
313	OPDX	0	1	3.54E-01	6.12E-01	0.00E+00	7.76E-02	-3.93E-01	8.47E-06
314	OPDX	0	1	4.71E-01	8.16E-01	0.00E+00	4.85E-02	1.19E+00	4.84E-05
315	OPDX	0	1	3.36E-01	0.00E+00	0.00E+00	4.85E-02	-5.60E-01	1.07E-05
316	OPDX	0	1	7.07E-01	0.00E+00	0.00E+00	7.76E-02	-3.93E-01	8.47E-06
317	OPDX	0	1	9.42E-01	0.00E+00	0.00E+00	4.85E-02	1.19E+00	4.84E-05
318	OPDX	0	1	1.68E-01	-2.91E-01	0.00E+00	4.85E-02	-5.60E-01	1.07E-05
319	OPDX	0	1	3.54E-01	-6.12E-01	0.00E+00	7.76E-02	-3.93E-01	8.47E-06
320	OPDX	0	1	4.71E-01	-8.16E-01	0.00E+00	4.85E-02	1.19E+00	4.84E-05
321	OPDX	0	1	-1.68E-01	-2.91E-01	0.00E+00	4.85E-02	-5.60E-01	1.07E-05
322	OPDX	0	1	-3.54E-01	-6.12E-01	0.00E+00	7.76E-02	-3.93E-01	8.47E-06
323	OPDX	0	1	-4.71E-01	-8.16E-01	0.00E+00	4.85E-02	1.19E+00	4.84E-05
324	OPDX	0	1	-3.36E-01	2.57E-16	0.00E+00	4.85E-02	-5.60E-01	1.07E-05
325	OPDX	0	1	-7.07E-01	5.41E-16	0.00E+00	7.76E-02	-3.93E-01	8.47E-06
326	OPDX	0	1	-9.42E-01	7.21E-16	0.00E+00	4.85E-02	1.19E+00	4.84E-05

327	OPDX	0	1	-1.68E-01	2.91E-01	0.00E+00	4.85E-02	-5.60E-01	1.07E-05
328	OPDX	0	1	-3.54E-01	6.12E-01	0.00E+00	7.76E-02	-3.93E-01	8.47E-06
329	OPDX	0	1	-4.71E-01	8.16E-01	0.00E+00	4.85E-02	1.19E+00	4.84E-05
330	OPDX	0	2	1.68E-01	2.91E-01	0.00E+00	4.85E-02	-6.41E-01	1.41E-05
331	OPDX	0	2	3.54E-01	6.12E-01	0.00E+00	7.76E-02	-3.77E-01	7.80E-06
332	OPDX	0	2	4.71E-01	8.16E-01	0.00E+00	4.85E-02	1.24E+00	5.31E-05
333	OPDX	0	2	3.36E-01	0.00E+00	0.00E+00	4.85E-02	-6.41E-01	1.41E-05
334	OPDX	0	2	7.07E-01	0.00E+00	0.00E+00	7.76E-02	-3.77E-01	7.80E-06
335	OPDX	0	2	9.42E-01	0.00E+00	0.00E+00	4.85E-02	1.24E+00	5.31E-05
336	OPDX	0	2	1.68E-01	-2.91E-01	0.00E+00	4.85E-02	-6.41E-01	1.41E-05
337	OPDX	0	2	3.54E-01	-6.12E-01	0.00E+00	7.76E-02	-3.77E-01	7.80E-06
338	OPDX	0	2	4.71E-01	-8.16E-01	0.00E+00	4.85E-02	1.24E+00	5.31E-05
339	OPDX	0	2	-1.68E-01	-2.91E-01	0.00E+00	4.85E-02	-6.41E-01	1.41E-05
340	OPDX	0	2	-3.54E-01	-6.12E-01	0.00E+00	7.76E-02	-3.77E-01	7.80E-06
341	OPDX	0	2	-4.71E-01	-8.16E-01	0.00E+00	4.85E-02	1.24E+00	5.31E-05
342	OPDX	0	2	-3.36E-01	2.57E-16	0.00E+00	4.85E-02	-6.41E-01	1.41E-05
343	OPDX	0	2	-7.07E-01	5.41E-16	0.00E+00	7.76E-02	-3.77E-01	7.80E-06
344	OPDX	0	2	-9.42E-01	7.21E-16	0.00E+00	4.85E-02	1.24E+00	5.31E-05
345	OPDX	0	2	-1.68E-01	2.91E-01	0.00E+00	4.85E-02	-6.41E-01	1.41E-05
346	OPDX	0	2	-3.54E-01	6.12E-01	0.00E+00	7.76E-02	-3.77E-01	7.80E-06
347	OPDX	0	2	-4.71E-01	8.16E-01	0.00E+00	4.85E-02	1.24E+00	5.31E-05
348	OPDX	0	2	1.68E-01	2.91E-01	0.00E+00	4.85E-02	-6.41E-01	1.41E-05
349	OPDX	0	2	3.54E-01	6.12E-01	0.00E+00	7.76E-02	-3.77E-01	7.80E-06
350	OPDX	0	2	4.71E-01	8.16E-01	0.00E+00	4.85E-02	1.24E+00	5.31E-05
351	OPDX	0	2	3.36E-01	0.00E+00	0.00E+00	4.85E-02	-6.41E-01	1.41E-05
352	OPDX	0	2	7.07E-01	0.00E+00	0.00E+00	7.76E-02	-3.77E-01	7.80E-06
353	OPDX	0	2	9.42E-01	0.00E+00	0.00E+00	4.85E-02	1.24E+00	5.31E-05
354	OPDX	0	2	1.68E-01	-2.91E-01	0.00E+00	4.85E-02	-6.41E-01	1.41E-05
355	OPDX	0	2	3.54E-01	-6.12E-01	0.00E+00	7.76E-02	-3.77E-01	7.80E-06
356	OPDX	0	2	4.71E-01	-8.16E-01	0.00E+00	4.85E-02	1.24E+00	5.31E-05
357	OPDX	0	2	-1.68E-01	-2.91E-01	0.00E+00	4.85E-02	-6.41E-01	1.41E-05
358	OPDX	0	2	-3.54E-01	-6.12E-01	0.00E+00	7.76E-02	-3.77E-01	7.80E-06
359	OPDX	0	2	-4.71E-01	-8.16E-01	0.00E+00	4.85E-02	1.24E+00	5.31E-05
360	OPDX	0	2	-3.36E-01	2.57E-16	0.00E+00	4.85E-02	-6.41E-01	1.41E-05
361	OPDX	0	2	-7.07E-01	5.41E-16	0.00E+00	7.76E-02	-3.77E-01	7.80E-06
362	OPDX	0	2	-9.42E-01	7.21E-16	0.00E+00	4.85E-02	1.24E+00	5.31E-05
363	OPDX	0	2	-1.68E-01	2.91E-01	0.00E+00	4.85E-02	-6.41E-01	1.41E-05
364	OPDX	0	2	-3.54E-01	6.12E-01	0.00E+00	7.76E-02	-3.77E-01	7.80E-06
365	OPDX	0	2	-4.71E-01	8.16E-01	0.00E+00	4.85E-02	1.24E+00	5.31E-05
366	OPDX	0	2	1.68E-01	2.91E-01	0.00E+00	4.85E-02	-6.41E-01	1.41E-05
367	OPDX	0	2	3.54E-01	6.12E-01	0.00E+00	7.76E-02	-3.77E-01	7.80E-06
368	OPDX	0	2	4.71E-01	8.16E-01	0.00E+00	4.85E-02	1.24E+00	5.31E-05
369	OPDX	0	2	3.36E-01	0.00E+00	0.00E+00	4.85E-02	-6.41E-01	1.41E-05
370	OPDX	0	2	7.07E-01	0.00E+00	0.00E+00	7.76E-02	-3.77E-01	7.80E-06
371	OPDX	0	2	9.42E-01	0.00E+00	0.00E+00	4.85E-02	1.24E+00	5.31E-05
372	OPDX	0	2	1.68E-01	-2.91E-01	0.00E+00	4.85E-02	-6.41E-01	1.41E-05
373	OPDX	0	2	3.54E-01	-6.12E-01	0.00E+00	7.76E-02	-3.77E-01	7.80E-06

374	OPDX	0	2	4.71E-01	-8.16E-01	0.00E+00	4.85E-02	1.24E+00	5.31E-05
375	OPDX	0	2	-1.68E-01	-2.91E-01	0.00E+00	4.85E-02	-6.41E-01	1.41E-05
376	OPDX	0	2	-3.54E-01	-6.12E-01	0.00E+00	7.76E-02	-3.77E-01	7.80E-06
377	OPDX	0	2	-4.71E-01	-8.16E-01	0.00E+00	4.85E-02	1.24E+00	5.31E-05
378	OPDX	0	2	-3.36E-01	2.57E-16	0.00E+00	4.85E-02	-6.41E-01	1.41E-05
379	OPDX	0	2	-7.07E-01	5.41E-16	0.00E+00	7.76E-02	-3.77E-01	7.80E-06
380	OPDX	0	2	-9.42E-01	7.21E-16	0.00E+00	4.85E-02	1.24E+00	5.31E-05
381	OPDX	0	2	-1.68E-01	2.91E-01	0.00E+00	4.85E-02	-6.41E-01	1.41E-05
382	OPDX	0	2	-3.54E-01	6.12E-01	0.00E+00	7.76E-02	-3.77E-01	7.80E-06
383	OPDX	0	2	-4.71E-01	8.16E-01	0.00E+00	4.85E-02	1.24E+00	5.31E-05
384	CONF	4	0	0.00E+00	0.00E+00	0.00E+00	0.00E+00	0.00E+00	0.00E+00
385	BLNK	0	0	0.00E+00	0.00E+00	0.00E+00	0.00E+00	0.00E+00	0.00E+00
386	LACL	0	0	0.00E+00	0.00E+00	0.00E+00	5.00E+07	0.00E+00	0.00E+00
387	SPHA	1	1	0.00E+00	0.00E+00	0.00E+00	5.00E+05	15.6E-04	38.3E+00
388	SPHA	1	2	0.00E+00	0.00E+00	0.00E+00	5.00E+05	12.3E-04	35.6E+00
389	EFFL	0	1	0.00E+00	0.00E+00	1.00E+00	5.00E+05	9.72E-01	2.84E-01
390	EFFL	0	2	0.00E+00	0.00E+00	1.00E+00	5.00E+05	9.70E-01	3.26E-01
391	AXCL	0	0	0.00E+00	0.00E+00	0.00E+00	5.00E+07	-8.86E-04	2.78E-02
392	MCOG	1	4	0.00E+00	0.00E+00	8.00E-02	7.00E+03	6.90E-02	5.99E-04
393	MXEG	6	7	0.00E+00	0.00E+00	5.00E-01	7.00E+03	2.94E-01	2.11E-01
394	MXEG	8	9	0.00E+00	0.00E+00	5.00E-01	7.00E+03	4.00E-01	4.95E-02
395	MXEG	10	11	0.00E+00	0.00E+00	5.00E-01	7.00E+03	6.90E-02	9.19E-01
396	BLNK	0	0	0.00E+00	0.00E+00	0.00E+00	0.00E+00	0.00E+00	0.00E+00
397	BLNK	0	0	0.00E+00	0.00E+00	0.00E+00	0.00E+00	0.00E+00	0.00E+00
398	OPDX	0	1	1.68E-01	2.91E-01	0.00E+00	4.85E-02	########	2.23E-04
399	OPDX	0	1	3.54E-01	6.12E-01	0.00E+00	7.76E-02	########	1.13E-04
400	OPDX	0	1	4.71E-01	8.16E-01	0.00E+00	4.85E-02	-6.19E-01	1.31E-05
401	OPDX	0	1	3.36E-01	0.00E+00	0.00E+00	4.85E-02	########	6.23E-04
402	OPDX	0	1	7.07E-01	0.00E+00	0.00E+00	7.76E-02	########	9.79E-04
403	OPDX	0	1	9.42E-01	0.00E+00	0.00E+00	4.85E-02	########	2.55E-04
404	OPDX	0	1	1.68E-01	-2.91E-01	0.00E+00	4.85E-02	########	1.06E-03
405	OPDX	0	1	3.54E-01	-6.12E-01	0.00E+00	7.76E-02	########	1.12E-03
406	OPDX	0	1	4.71E-01	-8.16E-01	0.00E+00	1.00E+00	5.40E-01	2.06E-04
407	OPDX	0	1	-1.68E-01	-2.91E-01	0.00E+00	4.85E-02	########	1.04E-03
408	OPDX	0	1	-3.54E-01	-6.12E-01	0.00E+00	7.76E-02	########	1.09E-03
409	OPDX	0	1	-4.71E-01	-8.16E-01	0.00E+00	1.00E+00	6.34E-01	2.84E-04
410	OPDX	0	1	-3.36E-01	2.57E-16	0.00E+00	4.85E-02	########	6.04E-04
411	OPDX	0	1	-7.07E-01	5.41E-16	0.00E+00	7.76E-02	########	9.14E-04
412	OPDX	0	1	-9.42E-01	7.21E-16	0.00E+00	4.85E-02	########	2.21E-04
413	OPDX	0	1	-1.68E-01	2.91E-01	0.00E+00	4.85E-02	########	2.17E-04
414	OPDX	0	1	-3.54E-01	6.12E-01	0.00E+00	7.76E-02	########	1.02E-04
415	OPDX	0	1	-4.71E-01	8.16E-01	0.00E+00	4.85E-02	-5.26E-01	9.47E-06
416	OPDX	0	1	1.68E-01	2.91E-01	0.00E+00	4.85E-02	########	2.23E-04
417	OPDX	0	1	3.54E-01	6.12E-01	0.00E+00	7.76E-02	########	1.13E-04
418	OPDX	0	1	4.71E-01	8.16E-01	0.00E+00	4.85E-02	-6.19E-01	1.31E-05
419	OPDX	0	1	3.36E-01	0.00E+00	0.00E+00	4.85E-02	########	6.23E-04
420	OPDX	0	1	7.07E-01	0.00E+00	0.00E+00	7.76E-02	########	9.79E-04

421	OPDX	0	1	9.42E-01	0.00E+00	0.00E+00	4.85E-02	########	2.55E-04
422	OPDX	0	1	1.68E-01	-2.91E-01	0.00E+00	4.85E-02	########	1.06E-03
423	OPDX	0	1	3.54E-01	-6.12E-01	0.00E+00	7.76E-02	########	1.12E-03
424	OPDX	0	1	4.71E-01	-8.16E-01	0.00E+00	1.00E+00	5.40E-01	2.06E-04
425	OPDX	0	1	-1.68E-01	-2.91E-01	0.00E+00	4.85E-02	########	1.04E-03
426	OPDX	0	1	-3.54E-01	-6.12E-01	0.00E+00	7.76E-02	########	1.09E-03
427	OPDX	0	1	-4.71E-01	-8.16E-01	0.00E+00	4.85E-02	6.34E-01	1.38E-05
428	OPDX	0	1	-3.36E-01	2.57E-16	0.00E+00	4.85E-02	########	6.04E-04
429	OPDX	0	1	-7.07E-01	5.41E-16	0.00E+00	7.76E-02	########	9.14E-04
430	OPDX	0	1	-9.42E-01	7.21E-16	0.00E+00	4.85E-02	########	2.21E-04
431	OPDX	0	1	-1.68E-01	2.91E-01	0.00E+00	4.85E-02	########	2.17E-04
432	OPDX	0	1	-3.54E-01	6.12E-01	0.00E+00	7.76E-02	########	1.02E-04
433	OPDX	0	1	-4.71E-01	8.16E-01	0.00E+00	4.85E-02	-5.26E-01	9.47E-06
434	OPDX	0	1	1.68E-01	2.91E-01	0.00E+00	4.85E-02	########	2.23E-04
435	OPDX	0	1	3.54E-01	6.12E-01	0.00E+00	7.76E-02	########	1.13E-04
436	OPDX	0	1	4.71E-01	8.16E-01	0.00E+00	4.85E-02	-6.19E-01	1.31E-05
437	OPDX	0	1	3.36E-01	0.00E+00	0.00E+00	4.85E-02	########	6.23E-04
438	OPDX	0	1	7.07E-01	0.00E+00	0.00E+00	7.76E-02	########	9.79E-04
439	OPDX	0	1	9.42E-01	0.00E+00	0.00E+00	4.85E-02	########	2.55E-04
440	OPDX	0	1	1.68E-01	-2.91E-01	0.00E+00	4.85E-02	########	1.06E-03
441	OPDX	0	1	3.54E-01	-6.12E-01	0.00E+00	7.76E-02	########	1.12E-03
442	OPDX	0	1	4.71E-01	-8.16E-01	0.00E+00	1.00E+00	5.40E-01	2.06E-04
443	OPDX	0	1	-1.68E-01	-2.91E-01	0.00E+00	4.85E-02	########	1.04E-03
444	OPDX	0	1	-3.54E-01	-6.12E-01	0.00E+00	7.76E-02	########	1.09E-03
445	OPDX	0	1	-4.71E-01	-8.16E-01	0.00E+00	1.00E+00	6.34E-01	2.84E-04
446	OPDX	0	1	-3.36E-01	2.57E-16	0.00E+00	4.85E-02	########	6.04E-04
447	OPDX	0	1	-7.07E-01	5.41E-16	0.00E+00	7.76E-02	########	9.14E-04
448	OPDX	0	1	-9.42E-01	7.21E-16	0.00E+00	4.85E-02	########	2.21E-04
449	OPDX	0	1	-1.68E-01	2.91E-01	0.00E+00	4.85E-02	########	2.17E-04
450	OPDX	0	1	-3.54E-01	6.12E-01	0.00E+00	7.76E-02	########	1.02E-04
451	OPDX	0	1	-4.71E-01	8.16E-01	0.00E+00	4.85E-02	-5.26E-01	9.47E-06
452	OPDX	0	2	1.68E-01	2.91E-01	0.00E+00	4.85E-02	2.41E+00	1.99E-04
453	OPDX	0	2	3.54E-01	6.12E-01	0.00E+00	7.76E-02	3.77E+00	7.78E-04
454	OPDX	0	2	4.71E-01	8.16E-01	0.00E+00	4.85E-02	4.78E+00	7.85E-04
455	OPDX	0	2	3.36E-01	0.00E+00	0.00E+00	4.85E-02	5.87E-01	1.18E-05
456	OPDX	0	2	7.07E-01	0.00E+00	0.00E+00	7.76E-02	7.16E-01	2.81E-05
457	OPDX	0	2	9.42E-01	0.00E+00	0.00E+00	4.85E-02	2.24E+00	1.73E-04
458	OPDX	0	2	1.68E-01	-2.91E-01	0.00E+00	4.85E-02	-8.39E-01	2.41E-05
459	OPDX	0	2	3.54E-01	-6.12E-01	0.00E+00	7.76E-02	-1.23E-02	8.27E-09
460	OPDX	0	2	4.71E-01	-8.16E-01	0.00E+00	4.85E-02	4.71E+00	7.61E-04
461	OPDX	0	2	-1.68E-01	-2.91E-01	0.00E+00	4.85E-02	-8.05E-01	2.22E-05
462	OPDX	0	2	-3.54E-01	-6.12E-01	0.00E+00	7.76E-02	5.89E-02	1.90E-07
463	OPDX	0	2	-4.71E-01	-8.16E-01	0.00E+00	4.85E-02	4.80E+00	7.91E-04
464	OPDX	0	2	-3.36E-01	2.57E-16	0.00E+00	4.85E-02	6.56E-01	1.47E-05
465	OPDX	0	2	-7.07E-01	5.41E-16	0.00E+00	7.76E-02	8.58E-01	4.04E-05
466	OPDX	0	2	-9.42E-01	7.21E-16	0.00E+00	4.85E-02	2.43E+00	2.03E-04
467	OPDX	0	2	-1.68E-01	2.91E-01	0.00E+00	4.85E-02	2.44E+00	2.05E-04

468	OPDX	0	2	-3.54E-01	6.12E-01	0.00E+00	7.76E-02	3.84E+00	8.08E-04
469	OPDX	0	2	-4.71E-01	8.16E-01	0.00E+00	4.85E-02	4.88E+00	8.16E-04
470	OPDX	0	2	1.68E-01	2.91E-01	0.00E+00	4.85E-02	2.41E+00	1.99E-04
471	OPDX	0	2	3.54E-01	6.12E-01	0.00E+00	7.76E-02	3.77E+00	7.78E-04
472	OPDX	0	2	4.71E-01	8.16E-01	0.00E+00	4.85E-02	4.78E+00	7.85E-04
473	OPDX	0	2	3.36E-01	0.00E+00	0.00E+00	4.85E-02	5.87E-01	1.18E-05
474	OPDX	0	2	7.07E-01	0.00E+00	0.00E+00	7.76E-02	7.16E-01	2.81E-05
475	OPDX	0	2	9.42E-01	0.00E+00	0.00E+00	4.85E-02	2.24E+00	1.73E-04
476	OPDX	0	2	1.68E-01	-2.91E-01	0.00E+00	4.85E-02	-8.39E-01	2.41E-05
477	OPDX	0	2	3.54E-01	-6.12E-01	0.00E+00	7.76E-02	-1.23E-02	8.27E-09
478	OPDX	0	2	4.71E-01	-8.16E-01	0.00E+00	4.85E-02	4.71E+00	7.61E-04
479	OPDX	0	2	-1.68E-01	-2.91E-01	0.00E+00	4.85E-02	-8.05E-01	2.22E-05
480	OPDX	0	2	-3.54E-01	-6.12E-01	0.00E+00	7.76E-02	5.89E-02	1.90E-07
481	OPDX	0	2	-4.71E-01	-8.16E-01	0.00E+00	4.85E-02	4.80E+00	7.91E-04
482	OPDX	0	2	-3.36E-01	2.57E-16	0.00E+00	4.85E-02	6.56E-01	1.47E-05
483	OPDX	0	2	-7.07E-01	5.41E-16	0.00E+00	7.76E-02	8.58E-01	4.04E-05
484	OPDX	0	2	-9.42E-01	7.21E-16	0.00E+00	4.85E-02	2.43E+00	2.03E-04
485	OPDX	0	2	-1.68E-01	2.91E-01	0.00E+00	4.85E-02	2.44E+00	2.05E-04
486	OPDX	0	2	-3.54E-01	6.12E-01	0.00E+00	7.76E-02	3.84E+00	8.08E-04
487	OPDX	0	2	-4.71E-01	8.16E-01	0.00E+00	4.85E-02	4.88E+00	8.16E-04
488	OPDX	0	2	1.68E-01	2.91E-01	0.00E+00	4.85E-02	2.41E+00	1.99E-04
489	OPDX	0	2	3.54E-01	6.12E-01	0.00E+00	7.76E-02	3.77E+00	7.78E-04
490	OPDX	0	2	4.71E-01	8.16E-01	0.00E+00	4.85E-02	4.78E+00	7.85E-04
491	OPDX	0	2	3.36E-01	0.00E+00	0.00E+00	4.85E-02	5.87E-01	1.18E-05
492	OPDX	0	2	7.07E-01	0.00E+00	0.00E+00	7.76E-02	7.16E-01	2.81E-05
493	OPDX	0	2	9.42E-01	0.00E+00	0.00E+00	4.85E-02	2.24E+00	1.73E-04
494	OPDX	0	2	1.68E-01	-2.91E-01	0.00E+00	4.85E-02	-8.39E-01	2.41E-05
495	OPDX	0	2	3.54E-01	-6.12E-01	0.00E+00	7.76E-02	-1.23E-02	8.27E-09
496	OPDX	0	2	4.71E-01	-8.16E-01	0.00E+00	4.85E-02	4.71E+00	7.61E-04
497	OPDX	0	2	-1.68E-01	-2.91E-01	0.00E+00	4.85E-02	-8.05E-01	2.22E-05
498	OPDX	0	2	-3.54E-01	-6.12E-01	0.00E+00	7.76E-02	5.89E-02	1.90E-07
499	OPDX	0	2	-4.71E-01	-8.16E-01	0.00E+00	4.85E-02	4.80E+00	7.91E-04
500	OPDX	0	2	-3.36E-01	2.57E-16	0.00E+00	4.85E-02	6.56E-01	1.47E-05
501	OPDX	0	2	-7.07E-01	5.41E-16	0.00E+00	7.76E-02	8.58E-01	4.04E-05
502	OPDX	0	2	-9.42E-01	7.21E-16	0.00E+00	4.85E-02	2.43E+00	2.03E-04
503	OPDX	0	2	-1.68E-01	2.91E-01	0.00E+00	4.85E-02	2.44E+00	2.05E-04
504	OPDX	0	2	-3.54E-01	6.12E-01	0.00E+00	7.76E-02	3.84E+00	8.08E-04
505	OPDX	0	2	-4.71E-01	8.16E-01	0.00E+00	4.85E-02	4.88E+00	8.16E-04